10. Nondestructive Evaluation

A. Nondestructive Inspection of Adhesive Metal/Metal Bonds

Principal Investigators:
Dennis Roach, Kirk Rackow, Ciji L. Nelson, Randy Duvall, David Moore
Sandia National Laboratories
P.O. Box 5800 MS 08635
Albuquerque, NM 87185
(505) 844-6078; e-mail: dproach@sandia.gov

Technology Area Development Manager: William Joost
(202) 287-6020; e-mail: william.joost@ee.doe.gov

Contractor: U.S. Automotive Materials Partnership
Contract No.: DE-AC04-94AL8500

Objective

- The goal of this project is to identify and develop one or more nondestructive inspection (NDI) methods for adhesive bond evaluation to be used in an automotive manufacturing environment that would foster increased confidence and use in adhesive joining. Wider use of adhesive joining could result in reduced vehicle weight, increased body stiffness, and improved crashworthiness.
- The primary objective is to identify and validate an NDI method(s) which can 1) measure the adhesive area and thickness, and 2) detect weak bonds having intimate contact but which have reduced strength. Adhesives are also seen as a critical enabler for the joining of dissimilar materials in order to avoid corrosion. To accomplish this goal, the attributes that determine bond strength were identified along with an NDI method to measure that property.

Approach

- There are five major attributes which contribute to the strength of an adhesive bond on a metal flange: the width of the adhesive area; the thickness; the location of the bead relative to the edges of the flange; the state of cure; and the quality of the adhesion. The general approach is to develop a portfolio of methods that can be used on the plant floor which allow all these attributes to be measured nondestructively.
- These methods need to be single-side inspections that can follow a flange, deal with large changes in geometry and have resolution approaching 1 mm. To accomplish this, several sets of flat adhesively bonded specimens, representative of automobile flanges, were generated by the original equipment manufacturers (OEM) and adhesive suppliers to test the feasibility of NDI techniques to assess bond area and bond-line thickness.
- The specimens vary in adhesive and adherent, type and thickness, stack-up (2-3 layers), and cure state. These conditions bound the processing parameters for the adhesive assembly

process. A through-transmission ultrasound (TTU) inspection was performed to characterize the specimens. The inspection images were used as a gold standard to compare results from candidate inspection technologies such as pulse-echo ultrasound and pulsed thermography which can be deployed from one side of the flange.

- The specimens were peeled destructively and photographs of the samples were also compared with the inspection images. In addition, multiple automobile bodies-in-white (BIW) containing a number of adhesive joints were produced by the OEMs to determine whether complex geometry produces any inspection impediments and to provide a test-bed for the validation of promising inspection techniques.
- Methods for producing weak bonds were developed and deployed to generate specimen sets for evaluating NDI ability to quantify bond strength.

FY 2009 Accomplishments

- The team completed the evaluation of the final, second generation array and probe holder (production prototype) on the BIW structures. This device is simpler and smaller than the first generation and should be able to inspect 95% of the BIW while imaging 85% of the area under the probe. The system works with a commercially-available closed-loop water circulation system and should have a significantly reduced system cost. The system is now at a production ready status.
- The BIW evaluations involved constructing inspection plans, inspecting over 100 beads with a wide variety of geometries and probe orientations, and generating evaluation reports. Over 80 % of the adhesive structure could be imaged at a speed of over 1 m/min with this feasibility system. These images elucidate large-scale features such as adhesive spread and the fill-factor of the flange. The 1 mm resolution also allows small features such as surface springback, air entrainment, bead dribbles, and weld expulsion damage to be imaged.
- An NDI method was developed for determining bond line thickness; an important quality assurance consideration for production. High fidelity pulse-echo ultrasonics, in conjunction with software to overlay signals from calibrated thicknesses, was used to measure and compare specific reflection peaks from within the adhesive joint. Validation on standard (0.4 mm), thick (0.6 mm) and thin (0.2 mm) bond lines established the ability of this method to accurately measure these thin adhesive layers to within 5%. Formal NDI procedures were produced.
- Reproducible procedures were established for constructing weak (kissing) bond samples using a wide variety of contaminates and controlled cures. Ten different methods were selected, based on repeatability of results, to produce specimen sets with 10%, 30%, 50%, 70%, 90% and 100% bond strength. Over 300 strengths tests were completed to characterize the weak bonds.
- NDI evaluations involving a suite of 9 inspection methods were completed on the weak bond specimens. Several methods clearly showed capabilities to delineate bond strength. NDI images could be correlated to the subsequent strength measurements. While the most sensitive NDI methods were not able to completely quantifying bond strength, they were able to accurately establish a strength threshold to indicate when the strength of the bond line falls below the 60-70% strength value.
- Tests were completed to quantify the effects of various bond line thicknesses and environmental exposure levels on the strength of the bonded joint. Both shear strength and fatigue (durability) tests established performance levels for standard, thick, and thin bond lines with and without extended exposure to hot-wet conditions.

Future Direction

- Fiscal Year (FY) 09 is the final year of this project. All deliverables and milestones have been met. Discussions with United States Council for Automotive Research (USCAR) participants indicates a desire to continue this work in a follow-on effort in order to complete the transfer of this inspection system to the automobile production line and to further the maturity of the weak bond quantification work.

Introduction

Adhesive bonding is an important joining tool for modern automotive structures. Structural adhesives can greatly increase the strength as well as stiffness of joints and can significantly improve the crash performance of vehicles. Structural adhesives also allow more efficient structures to be designed that may be difficult to weld. Structural adhesives will play an increasingly important role in the joining of dissimilar materials such as aluminum (Al) to steel or magnesium (Mg) to other metals: The adhesive acts both as a galvanic barrier and as a stress spreader on materials that are more brittle. The NDE 601 project was directed at filling a major technical gap for adhesives: how to determine whether an adhesive bond on a vehicle will perform as designed without actually destroying the bond. The major goal of this project was to develop an NDI method and associated system to inspect automotive flange joints: an ultrasonic pulse/echo inspection with a manually scanned phased array. A unique phased array probe system with a closed-loop circulation system was built by the team and successfully validated on numerous test coupons and production automobile bodies. Issues of inspection plan organization, report generation, accessibility, ultrasonic coupling, operator skill, and operator ergonomics were also evaluated. The system performed quite well delivering high resolution images of the adhesive area. Another issue critical to fabrication quality assurance is the ability to quantify the strength of the bonded joint. Once the team discovered methods to generate weak bonds in a controlled fashion, it was possible to study the ability of various NDI methods to characterize these weak bonds. It was shown that grease reduces both shear and tensile strength with the same sensitivity dependence and that grease contamination can be detected with ultrasonic pulse-echo inspections. Several NDI methods were developed with sufficient sensitivity to ascertain when bond strengths fall below 60% of full strength. Finally, it is important to be able to measure bond line thickness as variations from optimum designs can degrade strength and durability of the joint. This study proved the ability of an ultrasonic inspection method and associated signal analysis to accurately measure the thickness of a hidden bond line.

Nondestructive Inspection of Bond Lines and Bond Thickness Measurements

Phased Array Ultrasonic Inspections and Incorporation of Gen2 Scanning

The team completed the evaluation of the second generation ultrasonic array and probe holder that is intended as a production prototype (Figure 1). This device is simpler and smaller than the first generation and should be able to inspect 95% of the BIW while imaging 85% of the area under the probe. The system works with a commercially-available closed-loop water circulation system and should have a significantly reduced system cost. This inspection system was evaluated on three BIW structures. The BIW evaluations involved constructing inspection plans, inspecting over 100 beads with a wide variety of geometries and probe orientations, and generating evaluation reports. Images of the adhesive structure elucidate large-scale features such as adhesive spread and the fill-factor of the flange. The 1-mm resolution also allows small features such as surface springback, air entrainment, beads, dribbles, and weld expulsion

damage to be imaged. A formal inspection procedure was written and optimized during the trial inspections. Figure 2 shows a sample C-scan result with disbond flaws detected by the UT Array inspection system.

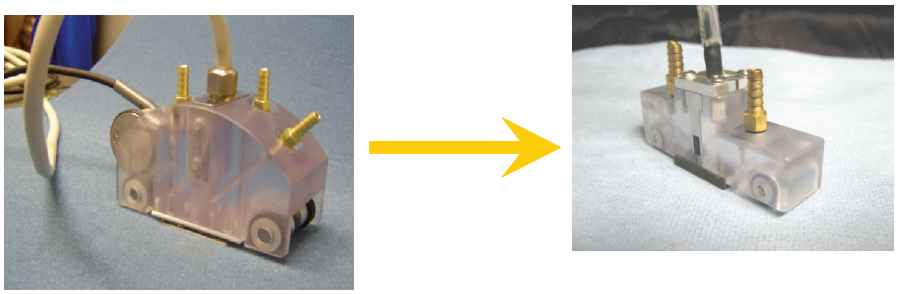

Figure 1. First generation (left) and second production-prototype generation (right) of the ultrasonic array and probe holder.

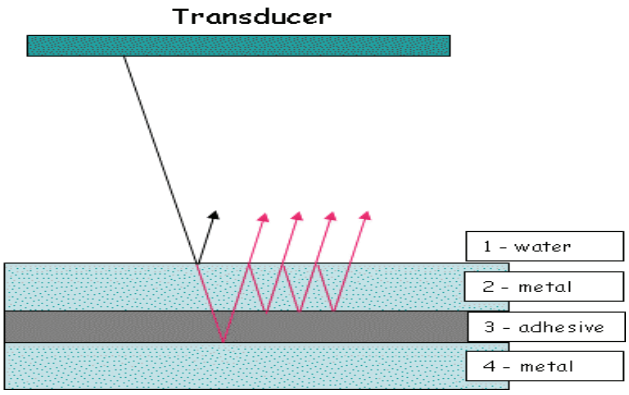

Figure 2. Phased array inspection of bonded joints in the BIW test articles and the resulting scans.

Ultrasonic Signal Analysis to Determine Adhesive Thickness

The signal-processing effort was completed to extract the adhesive thickness from the ultrasonic array echo data. This analysis can rapidly compensate for probe to surface distance variations. The short burst of high-frequency sound waves travel through the material with some loss of energy and is reflected at any interface. The reflected echo signal is captured and analyzed to determine the presence and location of reflected interfaces (Figure 3). Variations in reflectivity or scattering can be used as the basis of flaw detection. Transit times of the echoes can also be used to assess bond-line adhesive thickness. Two different adhesive thickness measurement methods were pursued. One NDI method produced spot measurements of adhesive layer thickness while the second method used the set of phased array A-scan/C-scan data to produce a thickness mapping of the entire bond line.

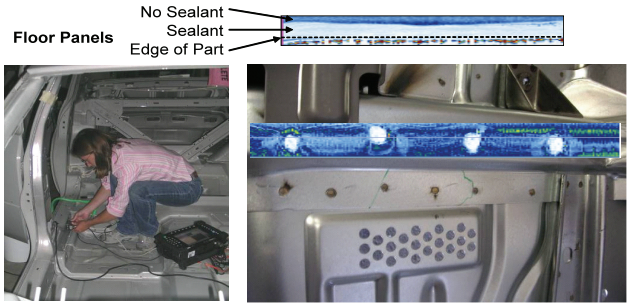

Figure 3. Ultrasonic set-up of the USCAR flange inspection.

Discrete adhesive thickness measurements were successfully produced using a Sonoscan C-SAM D9000 device shown in Figure 4. First, the acoustic velocity of epoxy adhesive was measured

and determined to be 2.345 mm/μsec. Then, the time lines for the critical echoes within the bonded joint, as depicted in Figure 3, were measured. These UT signals were overlayed with baseline signals from adhesive bond lines of known thickness. Using signal subtraction algorithms, the bond line thickness for all variations within the specimen set were determined. As it propagates through the layer to be measured, the ultrasonic energy is reflected at the front and back interfaces of the material. By measuring the time difference between the reflections, and factoring in the velocity of the ultrasound of the material, Sonoscan's software is used to intercompare signals and calculates the thickness of layers. Figure 4 shows the bond line thickness predictions produced by this UT peak signal inspection method and compares these results to those obtained from mechanical measurements. For bond lines that were intentionally varied +/- 50% from a desired thickness (0.2 mm to 0.6 mm), this method was able to accurately determine the bond thickness using pulse echo ultrasonic measurements to within 5% of actual thickness.

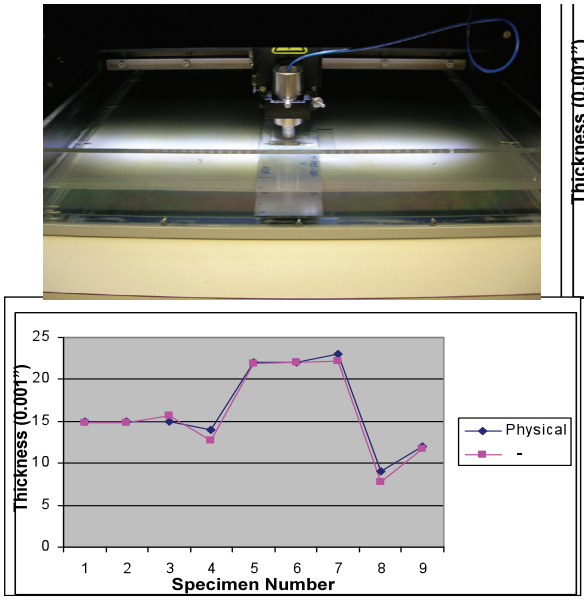

Figure 4. Sonoscan C-SAM D9000 pulse-echo ultrasonic inspection device and bond line thickness measurements produced using analysis of UT peak signals.

Nondestructive Characterization of Weak Bonds

A suite of customized applications of advanced NDI techniques, coupled with signal analysis, were applied to characterize bonds that are non-ideal and, thus, possess strengths that are less than optimum. The ideal result is data that can be calibrated to quantify the strength of a bond. Data analysis was used to highlight subtle changes in the structure's response and signal trends in order to link such differences to bond quality parameters. In order to obtain data that contains the small variation in bond line response, it was necessary to optimize the excitation used for the inspection. This includes both the frequency content and the magnitude of the excitation. Such optimization schemes considered the goal of keeping the inspections truly nondestructive; excessive excitation may damage the bond line. The source of the weak bond can stem from changes in the adhesive or a non-optimum interface between the adhesive and the adherend. This study focused on the expected sources of poor bonding at the adhesive-to-adherend interface. When assessing weak bonds, the source of the weak bond can stem from changes in the adhesive or a non-optimum interface between the adhesive and the adherend. One side aspect of this work determined if off-design cures produce changes in the material properties of the adhesives used in car production and to use NDI methods to monitor such

changes. By considering changes in the adhesive, these effects can be uncoupled in subsequent tests on bonded structures. Similarly, the effects of contaminants and other sources of weak bonds at the adhesive-to-surface interface will be studied. Results from mechanical property tests were intercompared and also compared with USCAR coupons of a different design. In this manner, NDI testing on the complete structure focused on the interface region to better identify/quantify a weak bond. The data analysis looked at subtle changes in the response and signal trends in order to link such differences to bond quality parameters

Generating Reliable Weak Bonds

The first challenge in this effort was to be able to create weak bonds with the adhesives used in the automotive industry in such a way that the strength results would be repeatable with some small level of variation. This was done by fabricating a series of lap joint coupons that are made of two galvanized steel adherends with a 1 inch overlap and a 1" x 1" bond area as shown in Figure 5. The thickness of the steel plate is 1.5 mm (0.060") and the thickness of the bond line is 0.40 mm (0.016"). The coupons were prepared using specific methods designed to produce various levels of weak bonds. The methods that were evaluated in this study included 30 different configurations and included: 1) various levels of grease thicknesses, 2) grease with thinner layers of adhesive, 3) different mold releases with various levels of coverage, 4) diluted mold release, 5) non-optimum cure profiles (varying in temperature and time), 6) hot-wet conditioning, 7) application of different contaminants (water, wax, sand, Vaseline), 8) oil application with various levels of coverage, 9) less than 100% adhesive coverage, and 10) baking powder with various levels of coverage. These specimens were then tested for strength by completing a failure test (tensile) in a uniaxial mechanical test machine. All the test results were collected and analyzed to determine the consistency (variance of strength), and the percentage of the full bond strength for each of the specific weak bond methods. It should be noted that a series of pristine coupons were fabricated in the same manner as the weak bond methods in order to provide strength and variance results for comparison purposes. The weak bond methods that showed the least amount of variance in strength results were then put into percentage of full strength bins (e.g. 10%, 30%, 50%). The final percentage of full strength bins used were 10%, 30%, 50%, 70%, and 90%. More coupons were fabricated and tested (strength tests) on the ten selected weak bond methods to insure repeatability (i.e. small deviation in strength). Table 1 shows the final selection of weak bond methods that were used for inspection purposes. Over 300 coupons were fabricated and tested to arrive at the final weak bond test set. Thus, there are 10 specimens in each NDI set with bond strengths in each of the following categories: 10% bond strength (2 types), 30% bond strength (2 types), 50% bond strength (2 types), 70% bond strength (2 types), 90% bond strength (1 type), 100% bond strength (1 type).

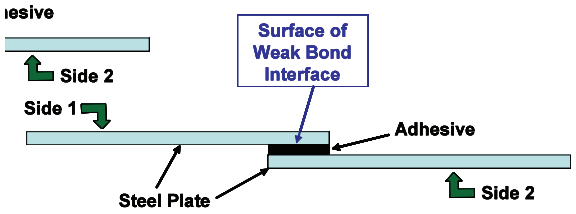

Figure 5. Weak bond lap splice test specimen.

Table 1. Summary of ten-specimen weak bond set.

Specimen No.	Description	No. of Strength Tests Completed	Avg. Strength (lbs./kN)	% of Bond Strength
T-PRI-7F-X	Pristine	10	3,349/14.9	100%
T-MO-RE-MS-25-zzF-X	Full Strength mold release (Miller-Steph. 25% cov.)	10	2,946/1	

Nondestructive Inspection of Weak Bonds

Based on previous experience in related weak bond studies, along with research into promising inspection methods, a suite of NDI methods was selected to study the weak bond specimens. The suite of NDI techniques evaluated were: 1) pulse-echo ultrasonics (UT), 2) phased array UT, 3) nonlinear UT, 4) UT spectroscopy, 5) resonance, 6) laser shot peening, 7) through transmission UT (immersion and air-coupled), 8) flash thermography, and 9) laser UT. Some techniques did not show any promise for assessing weak bonds, some techniques were able to identify the severely weak bonds (less than 20%), some techniques showed some trends but did not provide the resolution to make any clear indications of weak bonds and some methods clearly showed delineation in bond strength. The most promising and sensitive methods are described here.

While the most sensitive NDI methods were not able to completely quantifying bond strength, they were able to accurately establish a strength threshold. Inspection data often is presented in the form of C-scans which are two-dimensional, color or gray-scale coded plots where the colors correspond to assigned magnitudes in the NDI signals. Features revealed in the C-scans are able to indicate when the strength of the bond line falls below the 60-70% strength value. This is an important finding that provides the ability to more accurately and reliably establish accept-reject levels. Through-transmission ultrasonics was able to identify weak bonds. Figure 6 shows a series of amplitude plots along with the bond strength for each of the ten specimens in the weak bond set. These results show that the signal amplitude is affected by the physics of the changing bond and the general brightness of the C-scan darkens as the bond becomes weaker. The more field-deployable pulse-echo UT can also provide bond strength information using C-scan images produced after some custom signal analysis. Detailed analyses on pulse-echo ultrasonic signals was able to determine the portions of the signal that contained the primary bond strength information. These are highlighted as peaks 2, 3, and 5 in Figure 7. Focused analyses on these A-scan peaks produced some success in identifying weak bonds. The C-scans in Figure 7 show the results from using the change in the ratio of peak 3 to peak 2 and clearly demonstrates the promise for use of pulse-echo UT to quantify bond strength. In both cases the C-scan colors change from warm, bright colors to darker, cool colors as the bond strength degrades.

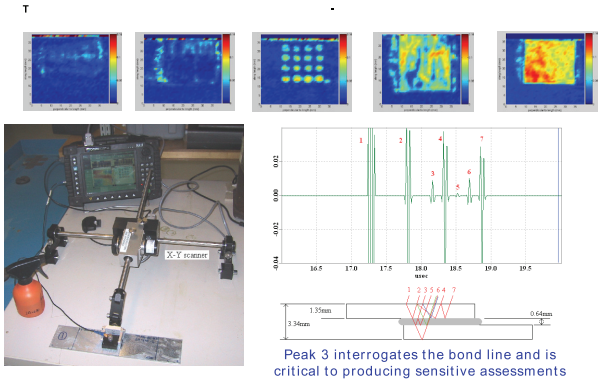

Figure 6. Tracing bond strength using through transmission ultrasonic images.

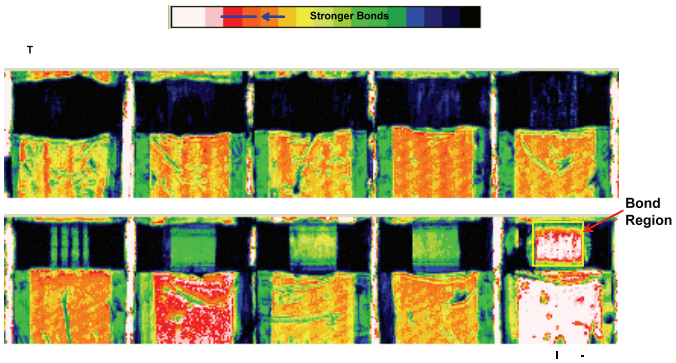

Figure 7. Pulse-echo UT inspections show promise for assessing bond strength using ratio of peak amplitudes.

The degree of variation in the C-scan images does not quite allow for exact bond strength values to be assigned based on the color codes. However, the images do significantly change when the bond strength drops to approximately the 60% (+/-) level. A-scan results from the weak bond specimen, such as the one depicted in Figure 7, show that the bond-related echoes 3, 5 and 6 are missing or reduced as the bond strength decreases. Thus, a measure of bond strength can be determined by calculating the ratios between the amplitudes of echo 2 in (steel travel only) and echo 3 in (bond line travel) for the array of specimens. Table 2 summarizes the results from this calculation and reveals that the UT peak signal measurements are close for 60-90% bond strength but can distinguish the bonds that are less than 50% (signal-to-noise levels are high enough to produce consistent results).

Other NDI methods were applied to fully exploit all characteristic features in bond strength inspections. Swept-frequency narrow-band spectroscopy has shown promise for improving the UT signal and an ability to differentiate low from high bond strengths. A dynamic modal testing method worked well when masses were added to the joints in order to uncouple the dynamic response of the “plate slapping mode” from the other specimen resonances. The natural frequencies decrease and the damping increases as the bond gets weaker. Laser peening methods were able to properly characterize the bonds in order of strength but the high energy levels required for inspection may deteriorate the bond. Shear wave resonance testing and thermography were able to differentiate high strength from low strength bonds when noise reduction schemes were deployed.

Figure 8 shows a series of thermographic images of weak bond specimens. Data acquisition software enhancements were used to filter the data and remove noise. In addition, flash quenching hardware was deployed to optimize the heat pulse excitation. The result is a much higher signal-to-noise ratio in the thermographic images and a greater sensitivity. This allows the bonds to be imaged differently, based on strength, and produces the set of images shown in Figure 8. Finally, resonance-based inspections monitored changes in acoustic impedance and were able

to image variations in the bond lines. Figure 9 shows the C-scan images from resonance testing which essentially uses an acoustic wave to interrogate the structure for stiffness variations. If the steel adherend is thin enough, resonance testing can detect changes in the strength of the bonded joint because the bond line plays a bigger role in the overall stiffness of the assembly.

Table 2. Identification of weak bonds using ratio of UT peak 2 and peak 3 amplitudes.

Sample	Bond strength %	Amplitude E3/amplitude E2
T-PRI-7F-G	100	0.096
T-MO-RE-MS-25-17F	88	0.085
T-GRE-100-01-21F-G	62	0.087
T-MO-RE-MS-50-18F-G	58	0.097
T-PWD-10-21F	46	0.024
T-SC-25-17F-G	46	0.016
T-PWD-25-21F-G	31	0.042
T-GRE-100-02-21F-G	26	0.014
T-GRE-100-05-21F-G	11	0.006
T-PWD-100-19F-G	10	0.01

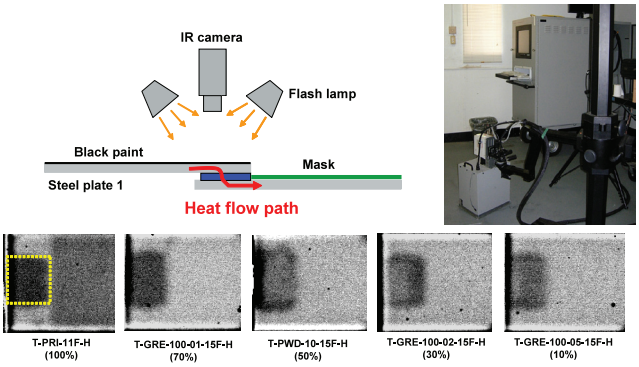

Figure 8. Thermography, coupled with signal optimization schemes, can differentiate bond strengths.

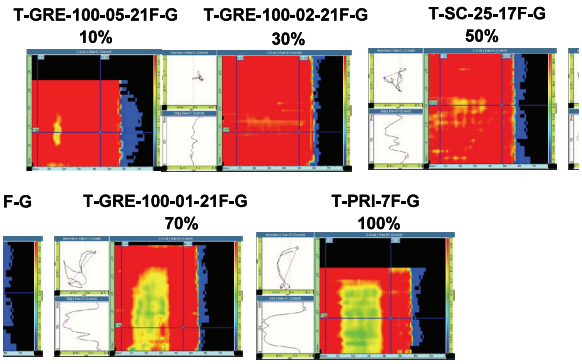

Figure 9. Resonance NDI method clearly shows when bond strength drops below 70% level.

Bond Strength and Durability Assessment

As an artifact of the weak bond study, it was also possible to evaluate the effects of various bond line thicknesses and environmental exposure levels on the strength of the bonded joint. A series of shear test specimens (see Figure 5) was produced to complete such a parametric study. In addition to the intentional weak bonds described above, the bond line thickness was studied in concert with the degrading exposure to hot-wet conditions (95% humidity at 140°F for 30 days). Both shear strength and fatigue (durability) tests were completed on approximately 10 coupons of each type. Figure 10 shows that the thin and thick bond lines possessed approximately the same shear strength as the standard, 0.4 mm bond line. Hot-wet exposure reduced the bond strength and the thin bond line was least affected by environmental

exposure. Fatigue test results showed that the thin bond (0.2 mm) exhibited the best durability results requiring almost six times as many fatigue cycles to produce failure as the standard bond line.

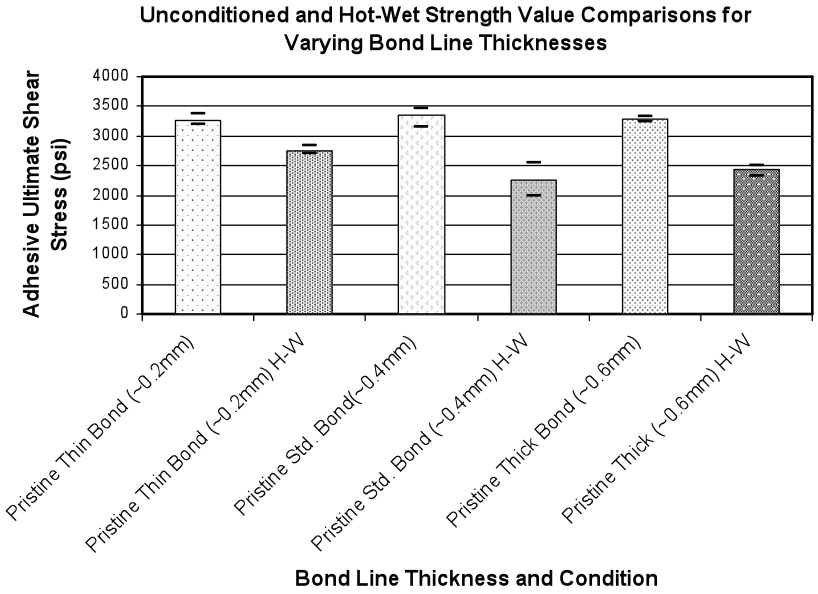

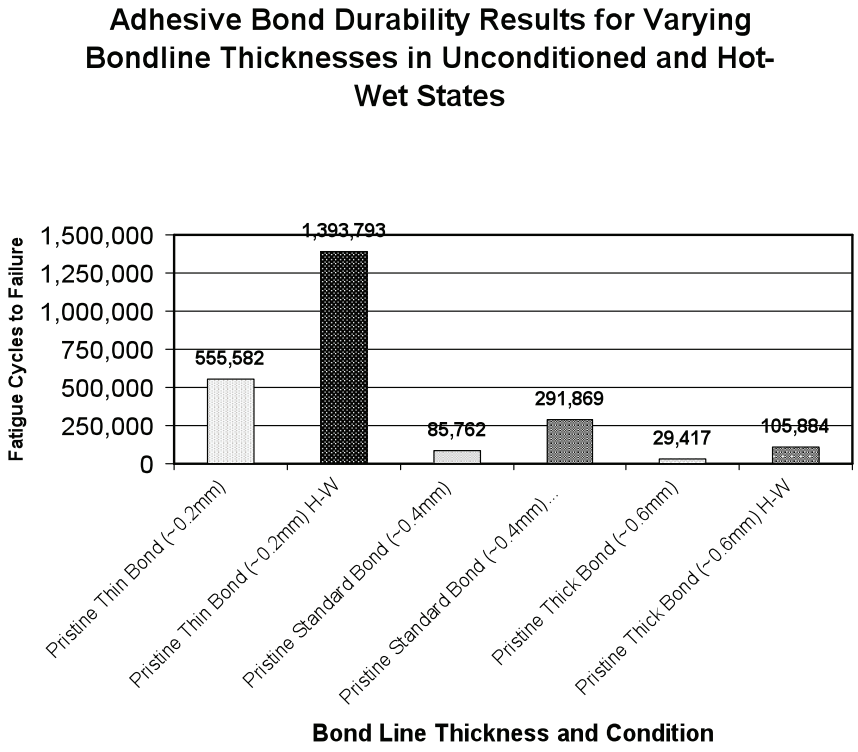

Figure 10. Strength and durability results for varying bond line thicknesses and effect of sustained hot-wet exposure.

Conclusions

FY2009 is the final year of this project. All deliverables and milestones have been met. The prototype production ultrasonic array tool for off-line inspections was successfully tested on production vehicles. The performance of this ultrasonic array system is adequate to allow the

adhesive mapping even on narrow flanges and on curved surfaces. This device is simpler and smaller than the first generation and should be able to inspect 95% of the BIW while imaging 85% of the area under the probe. The system works with a commercially-available closed-loop water circulation system and should have a significantly reduced system cost. The system is now at a production ready status. An NDI method was developed for determining bond line thickness. Validation on various bond lines established the ability of this method to accurately measure these thin adhesive layers to within 5%. The high-resolution wedge-peel test has been established as a bond strength standard. Simple scaling laws allow NDI measurements of bond width and thickness to predict the bond strength over a wide range of conditions. Ultrasonic NDI methods were developed to delineate bond strength. NDI images could be correlated to the subsequent strength measurements. While the ultrasonic-based NDI methods were not able to completely quantify bond strength, they were able to accurately establish a strength threshold to indicate when the strength of the bond line falls below the 60-70% strength value.

Presentation/Publications/Patents

- "Quantification of Weak Adhesion Using Nonlinear Ultrasonic Response Signals and Frequency Spectra," Drewry, M., Roach, D., Journal of Materials Evaluation, Vol. 67, No. 9, September 2009
- "Nondestructive Inspection of Adhesive Bonds in Automotive Metal/Metal Joints (NDE 601)," C. J. Dasch, USAMP Off-site Review, Oct. 29, 2008.
- "Ultrasonic Phased Array Tools for Large Area Composite Inspection During Maintenance and Manufacturing," Habermehl, J., Roach, D., Lamarre, A., Review of Progress in Quantitative Nondestructive Evaluation, Vol. 14, Plenum Press, New York, July 2008.
- "Using Quantitative Ultrasonic NDE to Accurately Predict Adhesive Bond Strengths," Cameron Dasch, Kim Lazarz, and Rajat Agarwal, Quantitative Nondestructive Evaluation Conference, Chicago, IL, July 2008
- "Correlating Adhesive Bond Strength with Non-Destructive Test Methods," K. Lazarz, C. Dasch, R. Agarwal, presented at the Annual Meeting of the Adhesion Society, Austin TX, Feb. 2008.
- Disclosure of Technical Advance Dated February 20, 2007, "Probe Deployment Device for Optimal Ultrasonic Wave Transmission and Area Scan Inspections," Joseph DiMambro, Dennis Roach, Kirk Rackow, Ciji Nelson, Sandia National Laboratories and Cameron Dasch General Motor Corporation.
- Roach, D., and DiMambro, J., "Enhanced Inspection Methods to Characterize Bonded Joints: Moving Beyond Flaw Detection to Quantify Adhesive Strength," Air Transport Assoc. Nondestructive Testing Forum, October 2006.

B. Laser Ultrasonic Inspection of Adhesive Bonds Used in Automotive Body Assembly

Principal Investigator: Marvin Klein
Intelligent Optical Systems
2520 West 237th Street
Torrance, CA 90505
Phone: (424) 263-6361; e-Mail: mklein@intopsys.com

Technology Area Development Manager: Carol Schutte
(202) 287-5371; e-mail: carol.schutte@ee.doe.gov

Contractor: Intelligent Optical Systems
Contract No.: DE-FG02-06ER84545

Objective

- Adhesive bonding is widely used in automotive production, especially for body assembly. It is critical to be able to measure the strength of adhesive bonds during manufacture in a nondestructive, effective and rapid manner. There are no current means for inspecting these bonds in real time. The specific inspection requirement is to (1) map the adhesive spread, (2) measure the thickness over the full area, and (3) measure the bond strength. All inspections must be performed from one side and must be able to function on contoured surfaces with ~1 mm resolution. The ideal tool must be able to perform the above measurements simultaneously (i.e., in one pass across the bond). In this project, we have applied the technique of laser ultrasonics to the adhesive- inspection requirements described above. The specific goals of this project are to determine the best inspection configuration and signal-processing approach, followed by the development and demonstration of a prototype inspection system.

Approach

- The technology which we have applied to this inspection requirement is laser ultrasonics, in which a pulsed laser beam is directed to the surface to generate ultrasonic waves in the sample, and a continuous-wave laser receiver is used to detect the waves after they interrogate the required sub-surface feature and return to the surface. Laser-based ultrasonic inspection has a number of benefits over transducer-based ultrasonic inspection, including: (1) lack of physical contact with the workpiece; (2) high spatial resolution obtained using focused laser beams; (3) high scan rate associated with rapid beam scanning; and (4) high bandwidth, thereby improving the measurement accuracy.

- This project has been closely coordinated with Sandia National Laboratories' phased-array project, "Nondestructive Inspection of Adhesive Metal/Metal Bonds," funded by the Department of Energy (DOE) and managed by the United States Council for Automotive Research (USCAR) Nondestructive Evaluation (NDE) Working Group (see 10.B). That USCAR-managed project has produced a large number of adhesive-bonded specimens. The flat specimens vary in adhesive, adherent type and thickness, stackup (2-3 layers), cure state, and surface contaminants. These conditions bound the processing parameters for the adhesive assembly process. These specimens have been used to optimize the beam configuration

and signal-processing techniques. The remaining portion of our project is devoted to the development and demonstration of a prototype scanning inspection system that can be scaled to a measurement speed of 1 meter/minute.

Accomplishments

- In 2009, we completed the remaining months of a 24-month Small Business Innovation Research (SBIR) Phase II project that started in 2007. During the course of this effort, we tested a number of steel and aluminum specimens prepared for the USCAR project, thus improving our ability to determine the configuration of both laser beams (separation, size, shape, energy) that provides the best signal-to-noise. We have identified techniques for processing the raw signals to provide accurate mapping of the adhesive spread and thickness, as well as to measure bond strength. Finally, we have designed a measurement head that is based on the required beam configuration, and delivered a full system using this head to General Motors.

Introduction

Adhesive bonding is widely used in automotive production, especially for body assembly. The most common use is the lap joining of two or three sheet-metal panels. Adhesive bonding adds strength, and thus allows the use of lighter components at equal performance. Adhesive bonding allows the joining of dissimilar materials such as aluminum (Al) and steel. Modern adhesives (especially epoxy resins) have excellent fatigue and thermal shock resistance, and less critical design tolerances because of their gap- filling capabilities. Their service range extends from space environments to high temperatures. It is critical to be able to measure the strength of these bonds during manufacture in a nondestructive, effective, and rapid manner.

The most important manufacturing issues that can influence the strength of an adhesive bond are the maintenance of the proper fit-up and proper surface preparation. While adhesive bonds are tolerant of some range of gap between the panels, if the gap is too large, the adhesive will not cover the required area, and the intrinsic strength of the adhesive itself is reduced. If surface contamination (e.g., oil, grease, surface oxides, corrosion, and water infiltration) is present, the bond adhesion will be reduced. In the limit of very low adhesion, weak bonds may have intimate contact, but little or no bond strength (“kissing”).

The corresponding requirements for nondestructive evaluation of adhesive bonds fall into three areas: (1) mapping of the adhesive coverage, (2) measurement of adhesive thickness, and (3) measurement of the adhesion of each metal/adhesive bond.

All inspections must be performed from one side and must be able to function on contoured surfaces. The ideal tool must be able to perform the above measurements simultaneously (i.e., in one pass across the bond).

At the current time, nondestructive inspection is not performed during the bonding process. The only quality control techniques now implemented are careful process control, machine-vision inspection of the adhesive bead before joining, and selective destructive evaluation. A nondestructive technique for in-line measurement of adhesive integrity would reduce scrap and warranty costs, and thus allow wider use of adhesive joining.

Laser ultrasonics offer an attractive approach for nondestructive evaluation over a broad range of applications. The full complement of ultrasonic waves (longitudinal, shear, Lamb, and Rayleigh) can be produced with known directionality. The pulses are high in bandwidth, thereby providing the high depth resolution required for thin sheets and bonds. The spot sizes on the part can be

much less than 1 mm in diameter, thereby providing high spatial resolution.

The objective of this project is to develop a real-time system for inspection of adhesive panels during auto body assembly (see Figure 1). This system will incorporate a fiber-delivered robotic measurement head containing a scanning mirror that will be able to scan narrow sections of adhesive very rapidly.

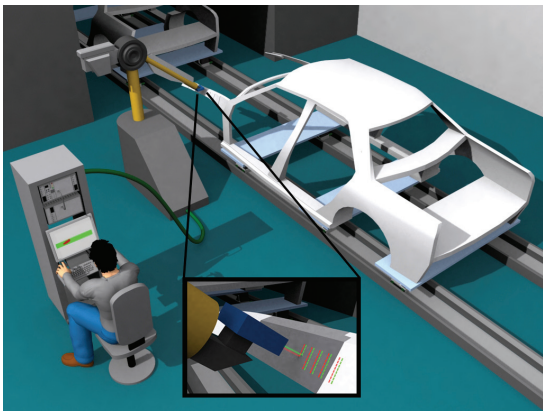

Figure 1. Depiction of robot-driven inspection system performing a two-dimensional scan of an adhesive-bonded auto body panel.

Adhesive Bond Strength Measurements

We next investigated a series of bond strength samples provided by Sandia National Laboratories. The samples were prepared with various bond strengths ranging from 10% to 100%. Our goal was to determine a suitable configuration, settings, and parameters of the laser ultrasonic inspection system, and a suitable bond strength metric applied to the laser ultrasonic data, which would enable the verification of existence or lack of adhesive, and the identification and classification of the samples according to their bond strengths. Several configurations of the generation lenses, including spherical, cylindrical, and cross cylindrical, with various focal lengths, were used for the experiments. The generation lens configuration proved to be the most critical factor for enabling the characterization of the adhesive samples. In particular, a single cylindrical lens with a focal length of 25 mm was determined to be the most effective. The beam separation and generation laser energy were also varied in the experiment, but were found to be not critical.

A set of oscilloscope time-traces were taken from four samples with different bond strengths, including on and off their adhesive regions. The beam separation was set at ~4.5 mm, and the time-span of the oscilloscope was set such that only the interface-echoes after the Rayleigh wave arrival and before the shock wave arrival were displayed. As an example, Figures 2 and 3 show the time-traces obtained from the sample with 26% bond strength over a time-span of 1.75 us to 4.25 us. The longitudinal-longitudinal (LL) echo separation is about 500 ns, and the time-trace contains 5 LL arrivals starting with the fourth echo, which is the first arrival appearing after the Rayleigh wave arrival.

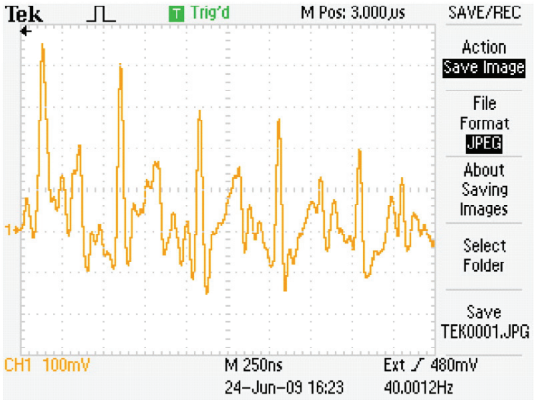

Figure 2. Off-adhesive time-trace for sample with 26% bond strength.

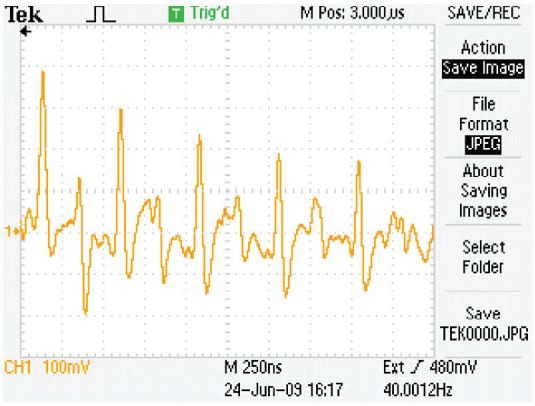

Figure 3. On-adhesive time-trace for sample with 26% bond strength.

As there was a high variation of surface reflectivity from sample to sample, and some surface variation within any given sample, including between its on-adhesive and off-adhesive regions, we selected the on-adhesive and off-adhesive inspected locations on a given sample such that the magnitude of the first arrival in the measured time-trace when on-adhesive is as close as possible to the magnitude when off-adhesive. Also, the arrivals after the shock wave were too weak to make meaningful measurements, even when the shock wave was set to arrive early. For a given sample, we observed that the ratios of magnitudes of adjacent interface-echo arrivals did not change appreciably when moving the laser beams across the sample. Comparing time-traces from samples with different bond strengths, we also observed a general trend of decreasing later arrivals with increasing bond strength for most of the samples. To quantify this effect, we selected and applied an algebraic metric to the peak magnitudes of the sequences of interface arrivals for the different samples. The result is shown in Table 1.

Table 1. Metric applied to time-trace data from samples with different bond strengths. In this table, "Arrival n" means the magnitude of the nth interface-echo LL arrival in units of mV.

Sample	Arrival 4	Arrival 5	Arrival 6	Arrival 7	Arrival 8	Metric
Bond 26%	380	300	230	180	170	0.58
Off-Adhesive	450	400	290	270	200	0.64
Bond 58%	195	140	80	75	80	0.48
Off-Adhesive	410	310	290	270	210	0.66
Bond 88%	390	180	175	130	130	0.39
Off-Adhesive	410	310	290	280	210	0.66
Bond 100%	83	63	52	48	36	0.6
Off-Adhesive	83	68	45	60	48	0.67

The metric is the summation of peak magnitudes of interface Arrivals 5 through 8, normalized by four-times the peak magnitude of interface Arrival 4. Since we start with Arrival 4 rather than with Arrival 1 for the calculation of the bond strength metric, the effect of large adhesive-interface ultrasonic-wave incidence-angles on the metric is minimized. Table 1 clearly demonstrates that: 1) the on-adhesive metric varies with bond strength; 2) for any given sample, the on-adhesive metric is lower than the off-adhesive metric; and 3) the off-adhesive metric is nearly the same for all four samples. The data also shows a monotonic decrease of the metric as the bond strength increases, for the samples with 26%, 58%, and 88% bond strengths. However, the sample with the bond strength of 100% did not follow this monotonic trend, and we are investigating whether this is caused by another characteristic of this particular sample besides its bond strength.

Prototype Development

We have developed a full laboratory prototype adhesive inspection system and delivered it to Cameron Dasch at General Motors R&D. The measurement head has been described in earlier Annual Reports. It is shown during target focusing in Figure 4.

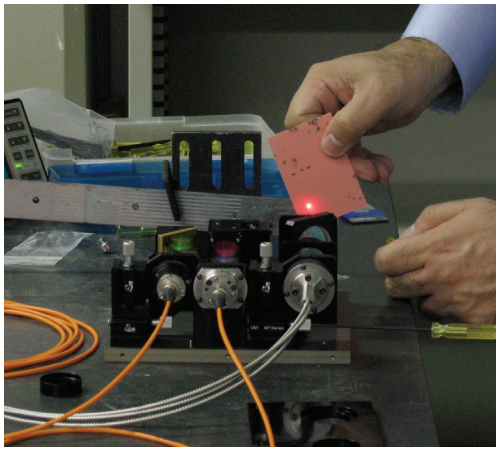

Figure 4. Focusing the measurement head during installation at General Motors. An adhesive sample is mounted as the target.

The head uses fiber delivery of the generation and detection laser beams to deliver spots on the target that have a controllable spacing and adjustable laser power/energy. The only connection to the measurement head is a fiber cable. A photo of the system during data acquisition is shown in Figure 5. Figure 6 shows a photo of the control equipment.

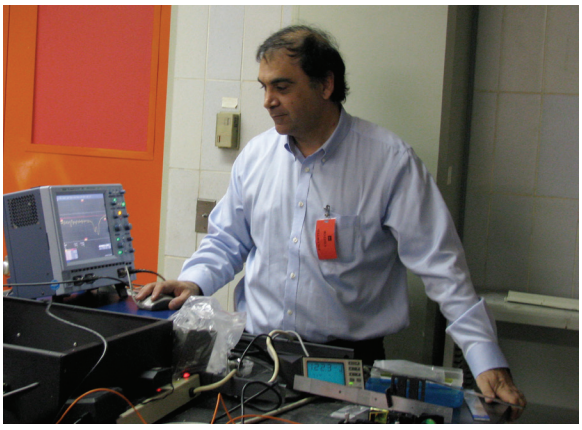

Figure 5. Acquiring data during the installation at General Motors.

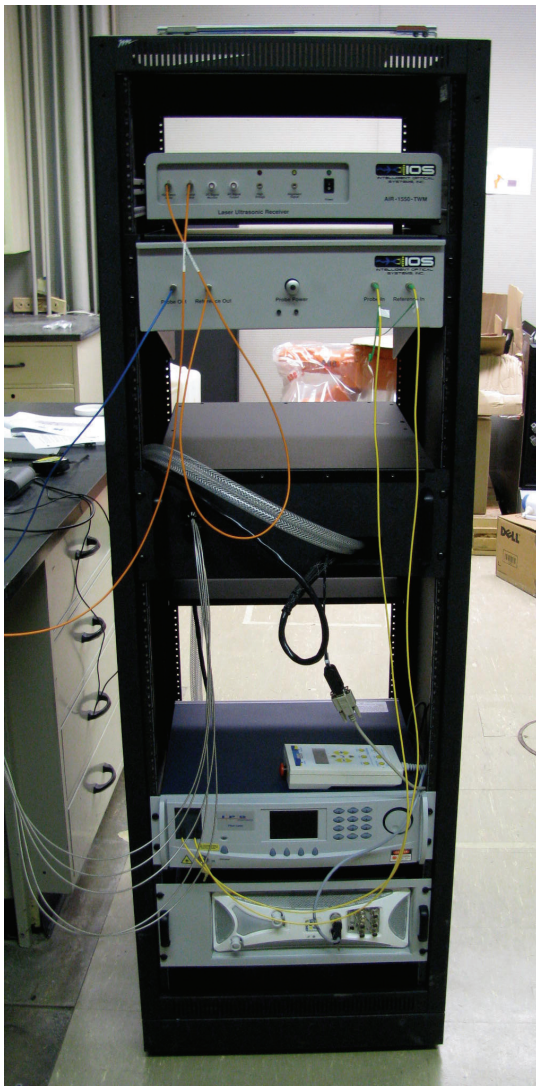

Figure 6. Control equipment.

Conclusions

In 2009, we completed this Phase II project. We have successfully applied laser ultrasonics to the requirements for evaluating adhesive bonds used in auto body assembly. Techniques have been developed to map the adhesive spread and measure the adhesive thickness. The signal processing efforts have indicated a pathway for processing the raw data in real time. We have designed and delivered a prototype scanning system to General Motors that will be robot-mounted for automated measurements. We have defined a pathway for measuring the adhesive bond strength.

Presentations/Publications/Patents

Marvin Klein and Homayoon Ansari, “Laser Ultrasonic Inspection of Adhesives Used in Auto Body Manufacture,” SAMPE 2010, Seattle, Washington, May 17-20, 2010.

C. On-Line Weld Quality Monitor and Control with Infrared Thermography

Principal Investigator: Zhili Feng
Oak Ridge National Laboratory
1 Bethel Valley Road, Oak Ridge, TN 37831
(865) 576-3797; e-mail: fengz@ornl.gov

Team Members:
Hsin Wang and Wei Zhang - Oak Ridge National Laboratory

Technology Area Development Manager: Dr. Carol Schutte
(202) 287-5371; e-mail: carol.schutte@ee.doe.gov

Field Technical Manager: C. David Warren
(865) 574-9693; e-mail: warrencd@ornl.gov

Contractor: Oak Ridge National Laboratory
Contract No.: DE-AC05-00OR22725

Objective

Develop an infrared (IR) thermography based weld quality detection technology capable of reliable and cost-effective on-line, non-destructive monitoring and feedback control of the welding assembly operation in a high-volume, automotive production environment.

- Phase I: Demonstrate the technical merit and potential of the IR based weld quality monitoring technology for resistance spot welds.
- Phase II: Field demonstration of a prototype system for real-time welding operation monitoring and on-line weld quality evaluation. This will include technology transfer and dissemination for future commercialization.

Approach

- Produce welds with different levels of quality and geometry attributes.
- Catalog and quantify weld quality attributes by means of destructive characterization.
- Develop quantitative correlation between various weld quality attributes and their characteristic IR thermal signature through combined welding heat flow simulation and laboratory IR experiments.
- Develop field-deployable IR measurement techniques for cost-effective detection of the characteristic thermal signature patterns during welding operation (real-time) and/or in on-line, post-mortem inspection.
- Develop efficient IR data analysis algorithms for thermal signature recognition.
- Integrate the field-deployable IR measurement system and the data analysis algorithm to develop a prototype IR weld quality monitor and control expert system for field demonstration.

Accomplishments

- We have successfully completed the Phase I Concept Feasibility study and demonstrated the feasibility and potential of both post-mortem and real-time IR thermography to detect weld quality and defects commonly encountered in resistance spot welds using industry practices.
- Major weld defect issues such as cold welds/stuck welds, weld expulsion, and unacceptable surface indentation are readily identifiable in both post-mortem and real-time IR measurements.
- The weld nugget size, a key weld quality measure governing the weld strength and failure mode in advanced high strength steel (AHSS) and other lightweight materials, can be deduced from both post-mortem and real-time infrared thermal image data.
- Other types of common weld defects such as cracking and void/porosity are detectable, although quantifying these defects requires further improvements in both IR image measurement techniques and detection algorithms.
- It is feasible for both post-mortem and real-time IR measurements to be performed online, and within 1-2 seconds.
- It is feasible to develop an IR image analysis expert software based on the artificial intelligence principle to determine the weld quality in real-time and without relying on operators skill and experience.

Future Direction

Phase II:

- Refine and optimize field-deployable IR measurement techniques that can reliably detect the characteristic thermal signature patterns of various weld quality attributes both in real time and in post-mortem, online inspection, including: (i) design and build a simple and cost-effective heating/cooling device for on-line post-mortem inspection; and (ii) evaluate the pros and cons of single-sided inspection vs. double-sided inspection.
- Develop robust IR image analysis software that, in real-time, can analyze the IR thermal image for the characteristic signature of various weld defects and weld joint configurations, to provide quantitative measure of the quality and the level of defects (if any) of spot welds of both steel and aluminum (Al) alloys.
- Identify a cost-effective IR imaging camera system that meets the on-line weld quality inspection needs.
- Develop a prototype IR weld quality monitoring expert system (hardware and software) for field demonstration.
- Identify potential industry entities for technology transfer and eventual commercialization.

Introduction

Welding is an essential technology used in automotive body structure assembly. Variations in welding conditions, materials, part dimensions and other production conditions inevitably occur in the high-volume and complex body-in-white (BIW) assembling process. These variations can result in “out-of-the-tolerance” welds that impair the quality and performance of the vehicles. Despite the extensive R&D efforts over the years, non-destructive weld quality inspection still remains a critical need in the auto industry, largely due to the unique technological and economical

constraints of the auto production environment. Any weld quality inspection technique must be fast, cost-conscious, low in false rejections, and not interfere with the highly automated welding assembly process.

Today, all OEMs primarily rely on destructive testing to ensure the integrity of critical structure members. Welded components are torn apart at predetermined time intervals (usually once per shift) to ensure the weld quality. The destructive testing is costly and labor intensive. As the teardown test cannot be done too frequently, the cost risk associated with reworking or scrapping the defective welded parts made between teardown tests is even higher. Furthermore, the teardown inspection techniques are less effective for advanced high-strength steels (AHSS), aluminum and other lightweight materials. As the industry moves toward body structures with more AHSS and aluminum, the post-mortem teardown inspection for weld integrity will be less reliable and more difficult and costly, potentially discouraging the implementation of these lightweighting materials.

In 2007, USAMP sponsored a study to assess the current status for in-line resistance spot welding (RSW) control and evaluation systems and to determine their application potential for lightweight sheet materials [1]. After extensive survey and communications with potential NDE suppliers and developers, the study concluded that "no economically reliable method exists today to inspect resistance spot welds at production rates, and the only technical needs identified in the project for further development consideration were in infrared thermography technology".

This project aims to develop a field-deployable, on-line weld quality monitoring method and a prototype system based on state-of-the-art IR thermography. A distinct advantage of IR thermography as a NDE tool is its non-intrusive and non-contact nature, making the IR especially attractive in hIR thermography detects surface temperature changes due to geometric discontinuity or inhomogeneity. An "out-of-tolerance" weld introduces a geometric change that would produce a perturbation of surface temperature profile from that of a normal weld. In theory, such temperature changes can be detected by IR thermography. In reality, detection of an anomalous weld by temperature change depends on many factors that can be grouped into four major categories: (1) factors inherent to the weld such as the heat flow characteristics of the weld, and the size, orientation, and location of the anomalous weld; (2) factors causing surface temperature changes unrelated to the presence of weld quality anomaly (such as emissivity changes due to changes in surface condition, reflection of other heat sources); (3) the sensitivity, spatial resolution, and other attributes of the IR measurement system; and (4) the detection algorithms – the ability to critically and effectively process the IR signals and positively identify an abnormal weld when present.

IR for weld quality inspection in the auto assembly environment has been explored in the past, mostly post-mortem (i.e. after weld is made and as a separate step in manufacturing). Typically, a short-pulse heating via xenon flash light (in a few milli-seconds) is applied to the surface of a spot weld. Temperature changes with time were then recorded by an IR camera and further processed to correlate to the weld size and other attributes of resistance spot welds. Such an approach had varying degrees of success in the laboratory environment and limited applications in other industries. However, applications in the automotive industry have been unsuccessful, largely due to a critical drawback that cannot be implemented in the high-volume production line which is the prerequisite of painting the weld surface to eliminate the surface reflection and other environment interferences [2].

1. Sun, X., Charron, W. Cerjanec, D., Bohr, J. and Cleaver, T. "AMD 605: In-Line Resistance Spot Welding (RSW) Control and Evaluation System Assessment for Light Weight Materials. (Final Report)," August 2008.
2. Communications with Weld NDE Subcommittee, Automotive Materials Partnership Steering Committee, USCAR, 2004.

Working with industrial partners, we recently demonstrated several novel concepts and approaches that would overcome some of the key technical barriers inhibiting the use of IR thermography as an effective weld NDE tool in the automotive assembly line. A unique advantage of the Oak Ridge National Laboratory (ORNL) approach is the potential for real-time weld quality detection as the weld is being produced. This would offer the opportunity of real-time welding process feedback for in-process adjustment and control [3].

This project builds upon recent work, and consists of a two-phase, gated R&D effort to further advance the IR thermography based weld quality monitoring and control technology to a stage that can be deployed in high-volume auto production environment. In this project, a two-phase, gated approach was adopted to develop an IR based weld quality inspection technology that overcomes the key technical barriers of the past. Phase I is a 12-month Concept Feasibility study to establish the technical basis and demonstrate the ability of detecting various types of defects (cold welds, cracking, expulsion, etc) and the critical weld quality attributes (weld size and indentation) in resistance spot welds produced using industry welding practices and without any surface treatment or preparation. Since it has been determined to be warranted, more comprehensive research and development program will be now be performed in the second phase (Technical Feasibility) toward eventual field demonstration of the technology.

The R&D in Phase I has been primarily carried out at ORNL, with support from the industry collaborators. An industry technical advisory committee has been formed for this project, consisting of representatives from Chrysler, Ford, General Motor, and ArcelorMittal.

Following the recommendations from OEM material joining and NDE experts and relevant USAMP AMD task teams, the project (Phase I and Phase II) includes tasks on both real-time weld quality monitoring and post-mortem weld quality auditing. The real-time monitoring is performed as a weld is being made, whereas the post-mortem auditing is performed as a separate step after welding. The two different techniques are needed to address different application situations. Both techniques must be suitable for on-line inspection.

Phase I consisted of three major milestones: (1) producing a limited set of controlled resistance spot welds having various types and levels of weld quality and defect attributes, and characterizing these weld attributes through destructive examination; (2) designing and performing IR measurements of these welds to obtain their “thermal signatures”; (3) IR data analysis and processing based on heat flow simulation to develop the correlation between the characteristic signature of IR images and the weld quality attributes.

Resistance Spot Weld (RSW) Samples for IR Thermography

In Phase I, a set of steel resistance spot welds were made having the typical range of weld defects and quality attributes known to potentially influence the structural performance of the spot welds in automotive body structures. These attributes are listed below, in the order of decreasing importance per the industry technical focus committee:

3. H. Wang,Z. Feng, and P.S. Sklad. (2004). “Inspection and Evaluation of Laser Welds for Transit Buses”. Thermosense XXVI, SPIE Defense and Security Conference, Orlando, FL.

- Weld with no or minimal fusion
- Cold or stuck weld
- Weld nugget size
- Weld expulsion/indentation
- Weld cracks
- Weld porosity

As a concept feasibility study, all welds were made on hot-dipped galvanized dual phase 780 MPa (DP590) steel of 1.85mm nominal thickness, in the common two-stack configuration. All welds were made at the Welding Lab of ArcelorMittal's research and development (R&D) Center in East Chicago, Indiana. For each welding condition, a total of six replicate welds were made. Two of the six replicates were sectioned destructively to determine the weld nugget size, type and degree of weld defects. The other welds of the same set were used in IR thermography measurements. In addition, extensive IR measurements were also conducted on one of the sectioned welds before it was sectioned. It was found those controlled welds made by ArcelorMittal were very consistent for a given welding condition. This greatly facilitated the development work in Phase I.

Table 1 summarizes the welds made with different quality attribute. Each weld was characterized by its nugget diameter, surface indentation, type and/or extent of defects. The weld nugget represents the fused region of the weld, and its diameter was determined using an optical microscope from both the cross-sectioned samples and the samples with one of the sheet steels carefully removed by machining and polishing to the faying surface of the weld. The table is color-coded. The second and third rows represent the welds acceptable in accordance with industry specifications, whereas the welds in the other rows are regarded to be "out-of-tolerance". Appearances of representative welds are shown in Figure 1 through Figure 5.

Table 1. Weld samples with different weld quality attributes produced at ArcelorMittal R&D.

Condition	Weld IDs	Weld Nugget Dia (mm)	Void Dia (mm)	Indent (mm)	Brassing	Cracking
Stuck Weld	34-39	0	None	0.06	None	None
Undersized weld	53-58	4.15	None	0.17	None	None
Minimum weld	65-70	5.8	None	0.21	None	None
Maximum weld	99-104	6.3	None	0.24	None	None
Void A	93-98	6.2	0.7	0.32	None	None
Void B	87-92	6.3	1.4	0.27	None	None
Expulsion/crack	117-122	7.4	None	0.62	None	None
Expulsion/crack	124-129	6.6	None	1.84	None	None
Expulsion/crack	131-136	6.6	None	1.04	Light	Yes
Expulsion/crack	138-143	7.9	None	1.72	heavy	Yes

Minimum weld refers to the minimum weld nugget diameter or button size perAWS specification. Maximum weld refers to the weld obtained using welding conditions just belowthe explosion limit.

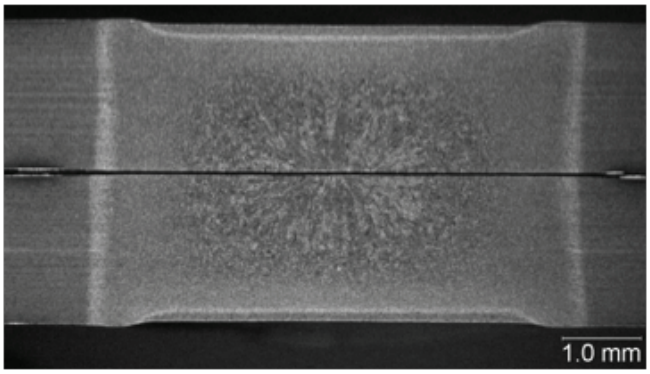

Figure 1. Cross-section view of a stuck weld with very small fused weld nugget.

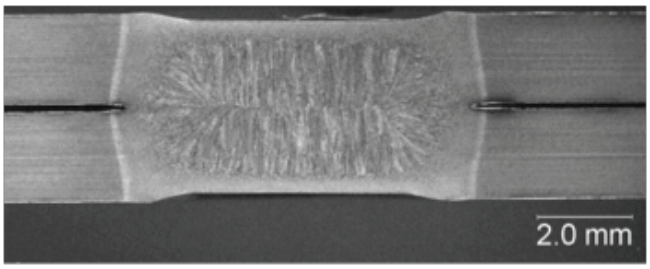

Figure 2. Cross-section view of a weld with acceptable weld nugget size and no defect.

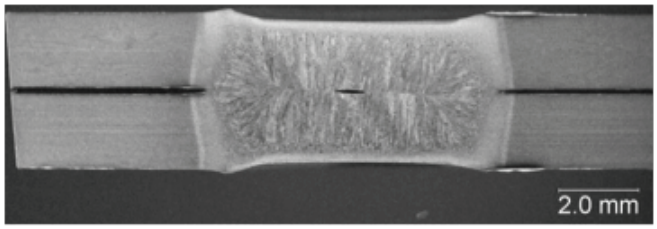

Figure 3. Welds with solidification shrinkage voids as revealed (a) in cross-section view and (b) by machining off one of the steel sheets.

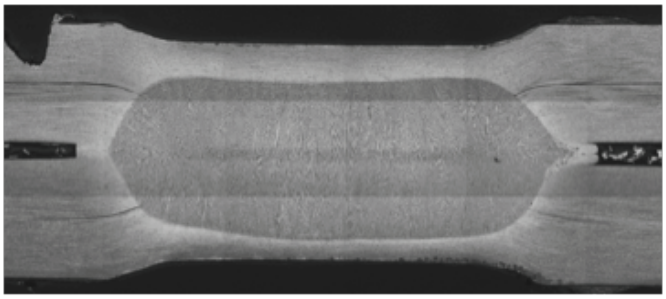

Figure 4. Cross-section view of a weld with expulsion.

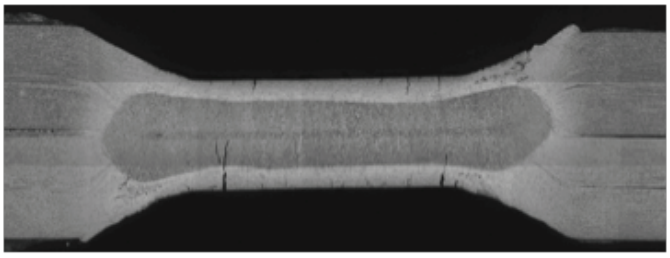

Figure 5. Cross-section view of a weld with expulsion, cracking and surface indentation.

Post-Mortem Inspection

Two types of IR weld quality inspections were studied in Phase I: postmortem and real-time. In all IR measurements, the weld sample surface was in as-welded condition – there was no any surface painting, cleaning or other treatments. Instead, the IR images were digitally enhanced during image analysis to minimize the effects of surface conditions (if any) encountered during either postmortem or real-time measurements. In addition, several heating/cooling techniques were tested and evaluated for enhancing the IR image signal to noise ratio.

In the post-mortem study, the IR measurement was conducted at ORNL on the welds made at ArcelorMittal. An external heating (or cooling) source was applied to introduce transient temperature changes in the weld and its surround area. An IR thermography camera was pointed to the weld surface to record the surface temperature changes. The measurement principle is illustrated in Figure 6.

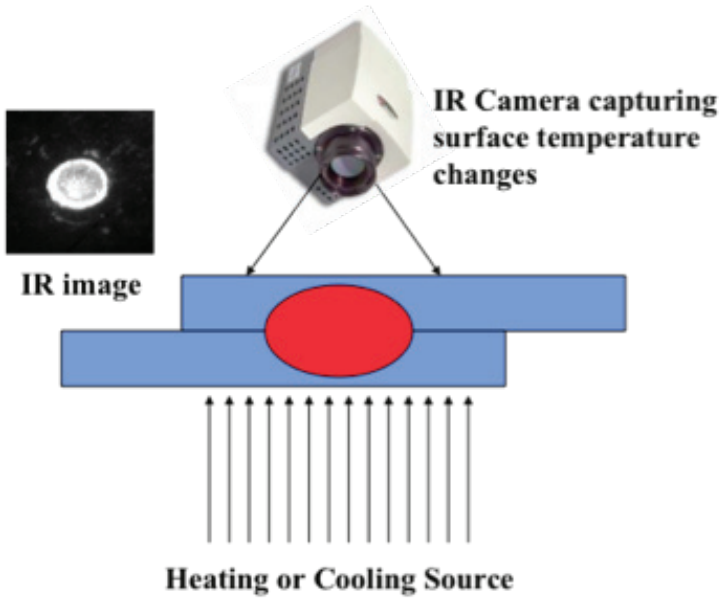

Figure 6. IR weld quality inspection principle (post-mortem approach).

The recorded IR images were then analyzed (offline and manually in Phase I) to obtain the characteristic thermal signature changes of the IR images and to relate such signature changes to the weld quality. The type of external heating or cooling source and the way it was applied influenced the heat flow in the weld and thereby the sensitivity and accuracy to detect the weld quality attributes. In Phase I, a total of six different heat and cooling techniques (three heating and three cooling) were evaluated. It was found that one heating technique and one cooling technique were particularly promising. They both required no physical contact between the cooling/heating device and the weld surface. The devices are readily available commercially, low-cost and highly portable. Together with the digital imaging enhancement techniques adopted in this project, these two techniques were capable of producing consistently clean signals (high signal-to-noise ratio) that facilitated the IR image analysis and correlation to the weld quality. These two promising techniques, herein referred to as the “ORNL heating or cooling methods”, are under internal review at ORNL for invention filing so details are omitted in this report.

The ORNL heating/cooling techniques were capable of producing very consistent results during repeated tests, and were able to distinguish major weld quality and defects in the controlled welds as shown in Figure 7. First of all, welds with different defects and geometry attributes have highly distinguishable temperature transient profiles. More encouragingly, the transient temperature curves can be roughly grouped into three distinct groups corresponding to the weld quality. The welds with the acceptable quality are in the middle band of the curves. The

welds with unacceptable quality attributes such as stuck welds, undersized weld (weld diameter less than the minimum specification by the industry), are clearly distinguishable from those of the acceptable welds. The welds with severe expulsion and cracking are distinctively located on the other side of the acceptable welds band.

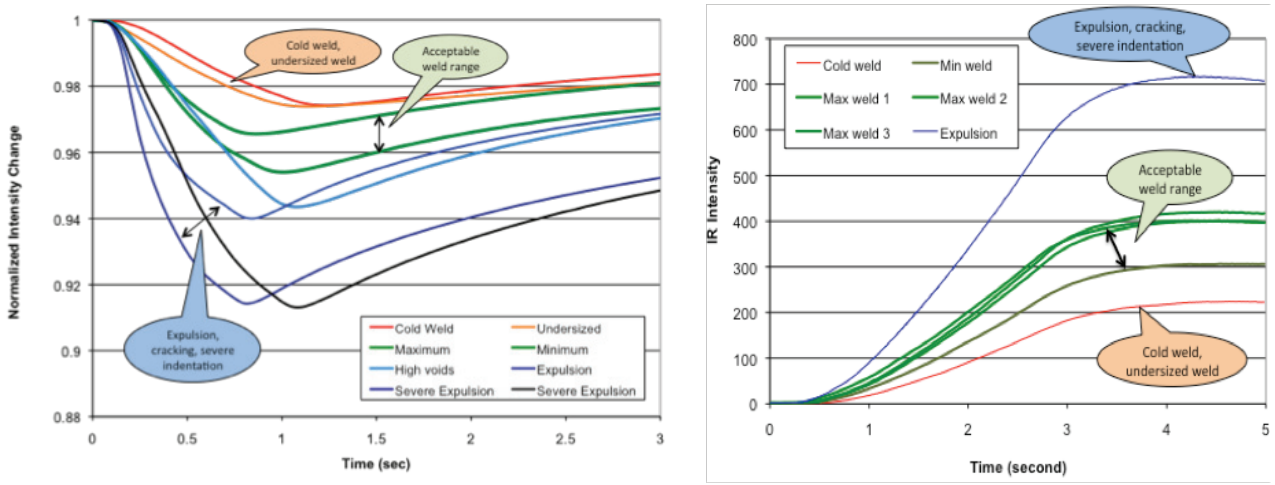

Figure 7. Post-mortem IR intensity curves of the controlled welds with different weld quality attributes, generated using the proprietary cooling technique (top) and proprietary heating technique (bottom). For each heating/cooling technique, identical IR image measurement condition was used for the welds with different quality/defect attributes, so that the differences in the recorded IR signal were solely from the variations in weld quality. The curves are color coded into three different groups corresponding to different weld quality attributes: (i) cold or undersized welds, (ii) welds within acceptable weld nugget size and minimum defects, and (iii) welds with detectable expulsion, severe surface indentation, and/or cracking.

Real-Time Inspection

Real-time IR inspection studies were performed on-site at ArcelorMittal R&D Center. A commercial IR camera (the same one used in the post-mortem study) was brought to the welding lab and used to capture the temperature changes during welding. The experimental set-up is shown in Figure 8, where an IR camera was placed near the spot welding head and pointed to the top surface of the spot weld.

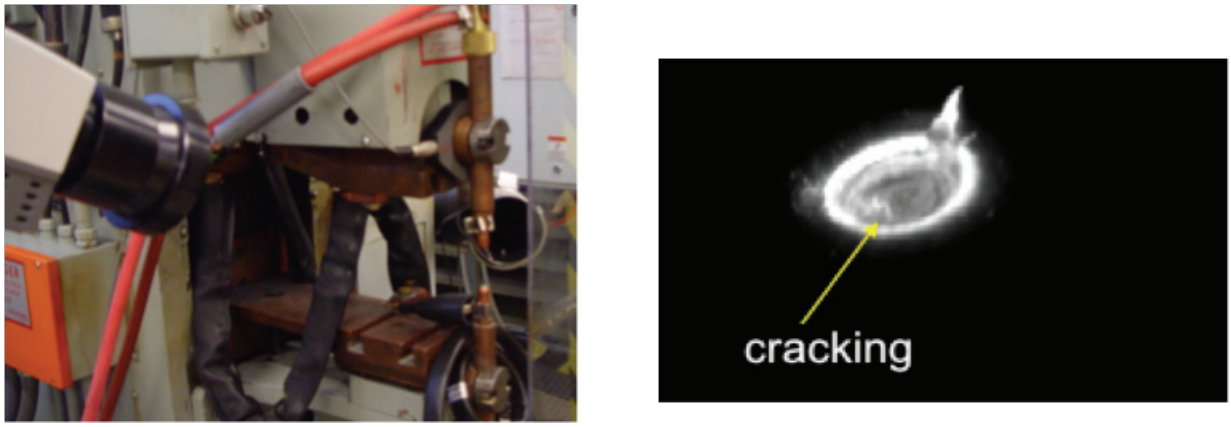

Figure 8. Real-time IR measurement set up and an IR image showing formation of a surface crack during welding.

The real-time IR measurement utilizes the heat generated during welding and the welding heat flow pattern changes caused by the formation of weld defects/anomalies or variations of weld geometric attributes (weld nugget size and surface indentation) to determine the weld quality as the weld is being produced. Examples of the real-time measurement results are given in Figure 9 in which three repeated IR measurements (on three separate welds) were performed for each welding condition. It is evident from the figure that the measurements for a given welding condition were highly consistent, and therewere definite correlations between the real-

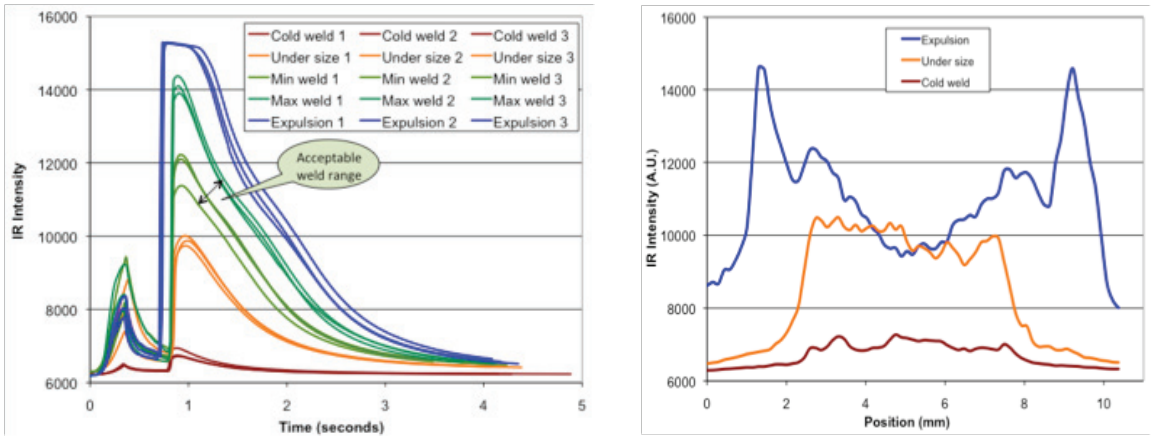

Figure 9. Real-time IR measurements of weld quality attributes. Top: IR intensity variations as function of time corresponding to different weld quality attributes. The real-time measurements were highly repeatable as indicated by three repeats for each welding condition. Bottom: line profile of IR intensity at a given time shows distinctive patterns associated with different weld quality attributes.

time IR signals and the different weld quality attributes for the weld studies in Phase I. This was consistent with previous work on laser welding [3]. In addition, surface cracks formed during welding were clearly visible during real-time IR measurement, as shown in the photo shown in Figure 8.

Initial Development of an Expert System

In Phase I, we also worked on a proof-of-concept development of the IR thermal signature analysis expert software for postmortem weld quality auditing. This expert software, to be fully developed in Phase II, aimed at providing reliable and accurate determination of the weld quality from the IR thermal signature measurements (either postmortem or real-time), without relying on the skills or experience of the operator (a major drawback prevented the use of IR inspection in the past). The software was based on the artificial intelligence principle and coded with generic signal pattern recognition routines. The initial proof-of-concept version was developed and evaluated with idealized post-mortem IR thermal profiles that were obtained from finite element simulation of the heat flow and surface temperature changes of welds with different nugget size and indentation features, under the heating conditions similar to the ORNL heating method developed in Phase I. Figure 10 shows the comparison of the prediction of the weld nugget sizes with the target ones. It is evident the feasibility of such software for weld quality determination.

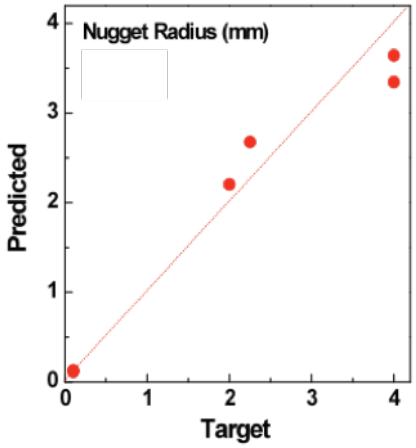

Figure 10. Demonstration of the artificial intelligence based expert software for weld nugget size detection (initial version in Phase I).

Cost/Benefit Analysis

Finally, we conducted a preliminary rough-order-of-magnitude (ROM) cost analysis of the IR based inspection system. The cost analysis included the cost of IR inspection head, the cost of robotic system, and the cost of labor and operation.

The IR inspection head consists of the IR camera, heating/cooling system for post-weld inspection, and the expert system software. According to a major IR camera manufacturer, a high performance camera capable of performing the type of full-field IR imaging in Phase I costs about $30K (camera and lens). This would be the upper end of the IR camera. It is noted that one of the major activities in Phase II is to refine and optimize the IR signal analysis algorithms to allow the use of low cost toolbox IR camera. A low cost IR camera currently cost under $15K and some are under $10K. Other IR head costs include: heating/cooling device for post-weld inspection (not needed for real-time monitoring), and the expert software. Induction heater: $8000; Liquid cooling: $1000; Software: $2,000. Therefore, ROM cost of the IR inspection head is in the range of $15K to $40K.

For on-line automated inspection, a robotic system is likely required. Since an IR camera only weights a few pounds, light duty robotics would be adequate. The cost of such systems is in the range of $30K to 50K, based on the information from OEMs and robotic manufacturers. Therefore, the ROM capital cost of the entire IR inspection system would be in the range of $45K to $90K.

Since the IR inspection system is highly automated and the expert system provides the visual feedback of weld quality and networked digital record archival, it is reasonable to expect that an operator for welding can be doubled for weld quality monitoring. In this case, the operating cost mostly consists of the cost of running the robotics, heating/cooling, and periodic inspection, calibration or maintenance of the IR camera head. From the technology perspective, the high labor cost (~$1M/year) in today's manual destructive pry-check and tear-down can be mostly eliminated. The ergonomic and safety issues in today's destructive inspection are also resolved. In addition, the automated IR inspection is expected to bring in significant cost savings from the reduced scrap and/or rework of defective welded parts associated with today's infrequent tear-down and pry-check.

Finally, today's teardown inspection techniques are less effective for advanced high-strength steels, aluminum and other lightweight materials. As the industry moves toward body structures with more AHSS and aluminum, teardown inspection for weld integrity will be less reliable and

more difficult and costly, potentially discouraging the adoption of these lightweighting materials. The IR based NDE technology, once successfully developed, would be a critical enabler for the widespread use of lightweight materials.

Conclusions

In Phase I, we evaluated approaches combining novel IR system setup and IR signal analysis techniques that have demonstrated the feasibility to overcome the key technical barriers inhibiting IR weld NDE in auto assembly line. Both post-weld inspection and real-time detection of weld quality were explored. The technical feasibility of IR NDE for weld quality and defect is summarized in Table 2. The post-weld approach was able to detect typical weld defects and determine the nugget size of steel spot welds. Furthermore, for the first time, the feasibility of real-time weld quality detection has been demonstrated. Both the post-mortem and the real-time approaches in Phase I required no special treatments of the as-welded or as-received surface – a key issue that has hindered previous IR attempts. As such, we have successfully met the milestones and passed the Technical Gate point set forth for Phase I.

Table 2. Feasibility of IR NDE of Weld Quality and Defects.

Weld Defect	Real-time	Post-weld
Fusion/No Fusion	Yes	Yes
Nugget Size	Yes	Yes
Stuck weld	Yes	Yes
Indentation	Yes	Yes
Expulsion	Yes	Yes
Porosity	> 0.2 mm	TBD
Cracking	> 1 mm	TBD

Future Directions

Phase II

- Refinement and optimization of field-deployable IR measurement techniques.
- User friendly IR image recognition expert software.
- IR weld NDE guideline for selected typical applications.
- Field demonstration and prototype systems.

Presentations/Publications/Patents

W. Woo, Z.Feng, H. Wang, C.W. Chin, W. Zhang, H Xu, and P.S. Sklad, “Application of Infrared Imaging for Quality Inspection in Resistance Spot Welds,” SPIE Defense, Security and Sensing Conference, April 13-17, 2009, Orlando, FL.

D. Enhanced Resonance Inspection for Light Metal Castings

Principal Investigator: Xin Sun
Pacific Northwest National Laboratory
Richland, WA 99352
(509) 372-6489; e-mail: xin.sun@pnl.gov

Technology Area Development Manager: William Joost
(202) 287-6020; e-mail: william.joost@ee.doe.gov

Field Technical Manager: Mark T. Smith
(509) 375-4478; e-mail: mark.smith@pnl.gov

Contractor: Pacific Northwest National Laboratory
Contract No.: DE-AC05-76RL01830

Objective

- To accelerate the development of rapid and reliable resonance inspection technique in ensuring the structural integrity of light metal castings.
- To assess the capability of modeling approaches in accurately predicting the vibrational mode frequencies along with the variability of those frequencies.
- To quantitatively evaluate the sensitivity of resonance inspection (RI) to anomalies of various types and sizes in various locations of a light metal casting.

Approach

- Develop a set of computational tools to enable predictive capability.
    1. Make current setup/training time shorter by using computer modeling to simulate response of actual parts and flaws.
    2. Identify response to critical flaws, thereby allowing “fault” to be specified and subsequently fixed (process feedback).
- Develop computational model to translate materials properties and geometry into predicted frequencies
    1. Use a Computer Aided Design (CAD) model or preferably three-dimensional (3D) scanning to provide exact as-is geometry to finite element analysis (FEA) model.
    2. Generate FEA 3D mesh directly from scanned data.
- Develop numerical algorithms to identify mode shapes for each frequency.
    1. Identify exact modal shapes for all the resonance frequencies in practical sampling range, i.e., 1 to 80 kilo-hertz (kHz). This is critical in determining what frequency changes correspond to which features in the part.
- Establish sensitivity matrix for critical anomalies.
    1. Use FEA to predict the response sensitivity to a specified feature (flaw) anywhere in the part.

2. Use perturbation theory-based numerical analyses to predict the frequency shift of a part, considering flaws at different locations.

- Validate modeling results by comparing predicted and measured frequencies and mode shapes.

1. Have multiple vendors collect data over full frequency range and compare these experimental measurements with FEA predictions.

Milestones, Metrics and Accomplishments

Completed RI testing on production part—a steering knuckle:

- Three vendors participated in the study.

Completed finite element simulations on the steering knuckle:

- Performed finite element-based natural frequency extraction.
- Performed mesh size convergence studies for the knuckle finite element model.
- Simulated actual RI experimental setup with steady-state dynamic simulation to obtain the vibrational amplitude at each resonant frequency.
- Calculated mode shapes and compared with experimental laser vibrometry measurements.
- Obtained good correlations between experimental frequencies to observed mode shapes.
- Predicted frequency shifts due to porosity and slits (oxide film model) using variational principles.
- Performed variational study to identify the influence of element density, stiffness, and part dimension on predicted natural frequencies and associated mode shapes.

Future Direction

- The project has been completed.
- The success of this project has led to a new project under U.S. Automotive Materials Partnership (USAMP) in developing the computationally enhanced RI sorting module.

Introduction

The resonance inspection (RI) technique is quick and very sensitive, making it an ideal choice in production environments.

Manufacturing acceptance of RI is limited by its empirical methodology and lengthy training period. In addition, the current RI technology does not provide any physics-based reasons for rejecting a particular part. The ability to use RI for testing and flaw identification has long been a desired inspection technology.

The goal of this concept feasibility project is to determine if it is feasible to use RI on a more quantitative basis by providing physics-based explainations of certain frequency shifts induced by flaws and anomalies. More specifically, we set out to assess the capability of finite element modeling approaches in accurately predicting the vibrational mode shapes and natural frequencies

along with the variability of those frequencies induced by structural flaws and anomalies. Possible benefits of the computationally enhanced RI technology include the following: decrease the required size of the training set; choose the frequencies to watch more intelligently; predict the sensitivity of the test to a specific feature, etc. Because of the complexity of the resonance structure in even simple parts, computer modeling of the RI process had previously been deemed as intractable in many instances.

In FY 2008, this project demonstrated that modeling the resonant behavior of simple parts is not only possible, but also quite accurate. We have compared the simulated results with the experimental results from two commercial vendors, The Modal Shop (TMS) and Magnaflux Quasar (Quasar). We have also shown that the use of laser vibrometry resolves any ambiguities as to the actual mode shape present at a particular frequency.

Based on the progress achieved during FY 2008 (Ref. 1, 2), FY 2009 has seen more achievements in both the experimental testing area and modeling area (Ref. 3). Great strides were also made in automating the mode identification process and in predicting accurate mode frequencies. Experimental resonance data have been collected on all the knuckles provided by our casting partner. We have also developed Finite Element Analysis (FEA) models from both Computer Aided Design (CAD) geometry and from computed tomography (CT) data in performing the subsequent natural frequency extraction analyses.

Variational principle-based formulations were also derived for quantifying the influence of part defects at different locations on the overall resonance of the knuckle. FEA models with defects have been created, and the result generated from the model provides some interesting comparisons with data from experiments. Study of the perturbation theory has also been extended.

FEA model for knuckle developed

An automotive steering knuckle, as shown in Figure 1, has been chosen as a production part for our study. Commercial finite element software ABAQUS (Ref. 4) is used. FEA models have been created from both CAD geometry and CT scan data.

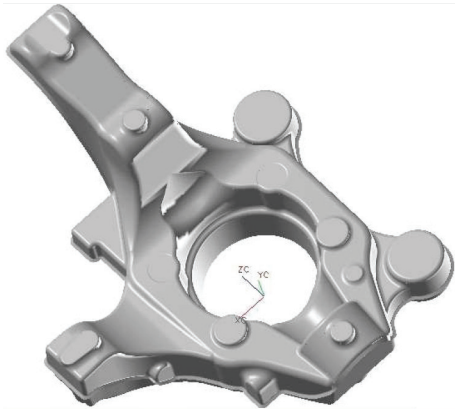

Figure 1. An automotive steering knuckle chosen for our concept feasibility study.

Figure 2 shows the measurable geometry difference between the CAD model and the CT scan result of the sample knuckle part. In some areas, the difference of two models can be as much as 6 mm. Consequently, the predicted frequency spectra for the two models are also slightly different.

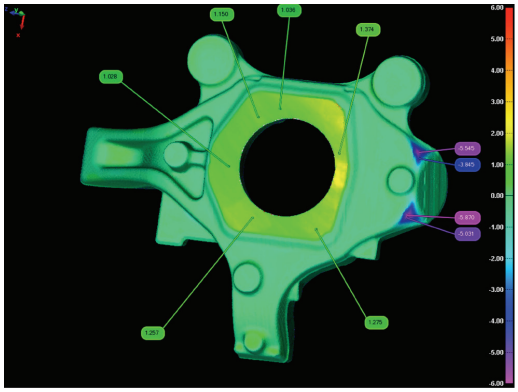

Figure 2. Geometry discrepancy between the CT model and the CAD model.

Mesh size convergence

A mesh size convergence study was carried out by running the finite element frequency extraction with different characteristic mesh sizes ranging from 2.0 mm to 0.8 mm. By comparing results from models with different mesh sizes, the following observations on mesh size convergence can be made:

In general, predicted natural frequencies for every mode decrease as mesh size decreases. An extrapolation curve fitting can be used to estimate the convergent resonance frequencies with a sufficiently small mesh size.

The converged mesh size can be established as the largest mesh size below which no more mode switches can be predicted when mesh size is further reduced.

Comparison of predicted and measured resonance frequency spectra

Very good comparison has been achieved between the experimentally measured and FEA predicted resonance spectra for the steering knuckle with mesh size of 0.8 mm. Figure 3 illustrates the comparison for the first 20 kHz. In Figure 3, the peaks above the x-axis are the experimentally measured resonance spectra with the response power at different frequency levels, and “HT” stands for “heat treated” in the legend of Figure 3.

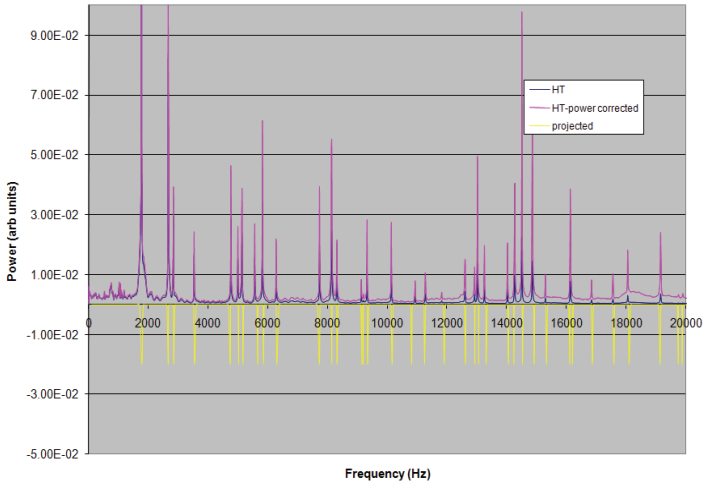

Figure 3. Comparison of resonance frequencies for the first 20 kHz from TMS experiments and ABAQUS simulation.

The peaks below the x-axis are the predicted resonance at different frequency levels. Since the natural frequency extraction analysis does not provide any response amplitude, the predicted results are plotted with uniform magnitude. The good alignment between the top experimental spectrum and the lower predicted spectrum demonstrates that finite element-based modal analysis can be used to accurately predict the natural frequency response of a production-level light metal casting part.

Complete mode shape catalog

The vibrational mode shapes for the lowest 100 frequencies have been plotted and cataloged from the ABSQUS FEA results based on a CAD part. As an illustration, Figure 4 shows the mode shape for No. 88 with a natural frequency of 37098 Hz for the steering knuckle.

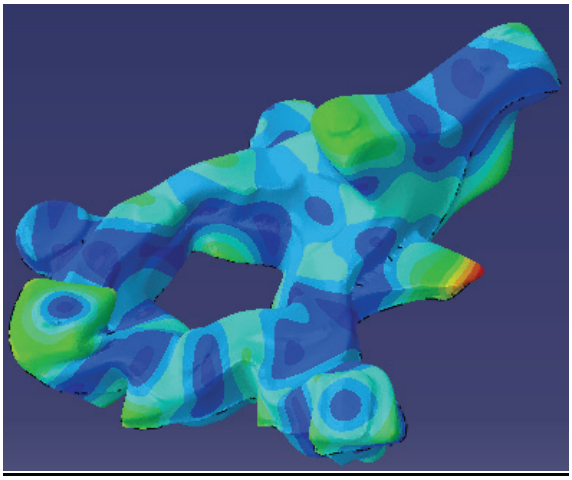

Figure 4. Knuckle mode shape at 37098 Hz.

Comparison of mode shapes predicted by FEA with those measured by Laser vibrometry

Experimental-mode shape measurements for the knuckle have also been performed using laser vibrometry by Polytec, a commercial supplier of this technology. Polytec measured the actual motion of the parts as they were being acoustically excited. Because of the size of the knuckle, for each frequency, a total of 10,000 scanned points divided into 21 image groups was used to cover the whole surface of the knuckle. The scan frequency of 5 Hz was used to minimize the size of the scan data file.

An automated mode shape matching algorithm between FEA prediction and experimental measurements has been developed and implemented, which has greatly reduced the human error in mode matching. A resemblance coefficient ranging from 0 to 1 is calculated between a Polytec mode and a predicted mode (Ref. 3). A coefficient close to 1 indicates perfect matching of the mode pair. For example, Figure 5 shows the experimentally measured mode shape at a resonance frequency of 16810 Hz, and Figure 6 shows the corresponding mode shape predicted by the finite element analysis. For this pair, the resemblance coefficient is 0.87.

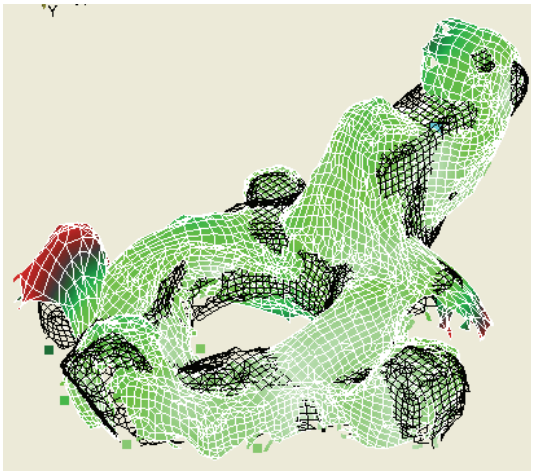

Figure 5. Polytec-measured knuckle vibrational mode shape at F=16810 Hz. Red region represents highest absolute displacement.

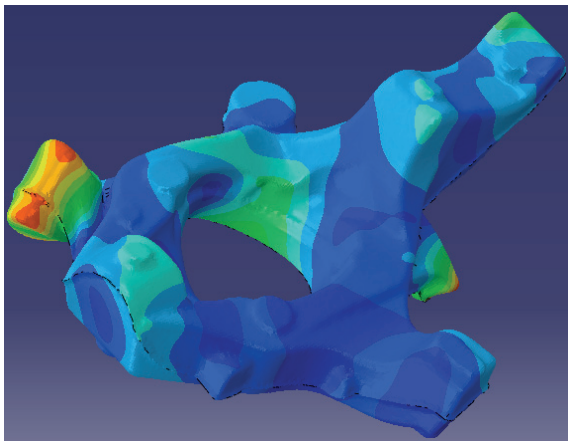

Figure 6. Knuckle mode shape at 16825 Hz as generated from ABAQUS FEA model. Region at left side represents highest absolute displacement.

Variational study on influences of density, stiffness, and part dimension on resonance frequency

A perturbation theory-based variational approach has been used to derive the analytical resonance frequency shift due to a small change in part density, material modules, and/or part geometry. It is shown that the frequency shift for each mode is proportional or inversely proportional to the changes in density, ρ, stiffness, E, and overall geometry scale, V.

Subsequent finite element analyses were performed, and the predicted frequency shifts match well with the perturbation theories (Ref. 3):

$$\frac{\Delta f}{f} = -0.5\frac{\Delta \rho}{\rho}; \frac{\Delta f}{f} = 0.5\frac{\Delta E}{E}; \frac{\Delta f}{f} = -\frac{\Delta V}{3V}$$

Steady-state dynamics analyses for the knuckle

In addition to the modal analysis, steady-state dynamic analyses were also performed for the knuckle to predict the relative magnitude of each resonant frequency.

This is done by exciting the steering knuckle at a certain frequency with a concentrated force applied at the driver node (see Figure 7), along with a uniform gravity force acting on the whole part. A boundary condition of zero displacement at the thickness direction is applied to the two nodes representing the two receiving transducers in the experimental setup. A steady-state dynamics analysis is run after the linear frequency extraction step. The reaction force is obtained at the two transducer nodes, and the response power is calculated as the average reaction force from the two nodes.

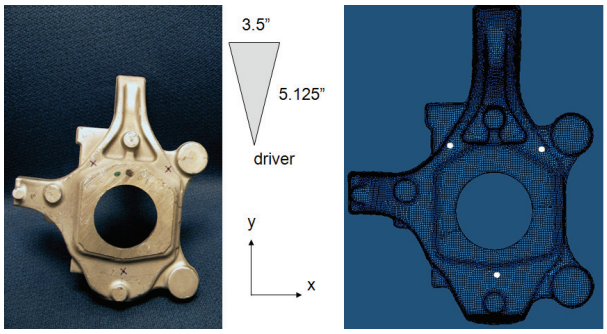

(a) (b)

Figure 7. Illustration of the transducer locations for the knuckle for (a) experiment—see black X on part (b) steady-state finite element analysis—see white dots on part.

Figures 8 and 9 compare the predicted vibration magnitude at each frequency level with the experimental measurements. Here the Quasar data are shown with a real power unit, and the ABAQUS results are plotted with their relative values in negative for each frequency. Relatively good resonance magnitudes have been obtained in comparison with the Quasar experimental data, particularly for the 20 kHz - 40 kHz range.

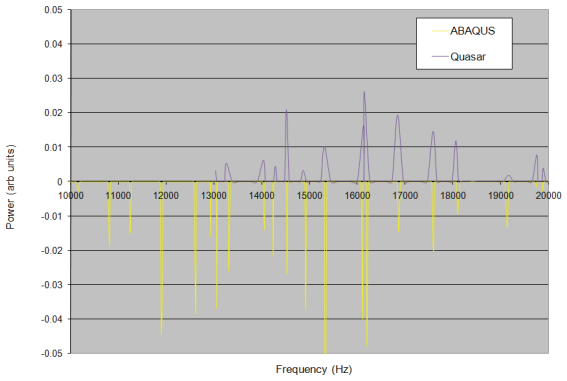

Figure 8. Steady-state dynamics comparison for the first 20 kHz resonance frequencies.

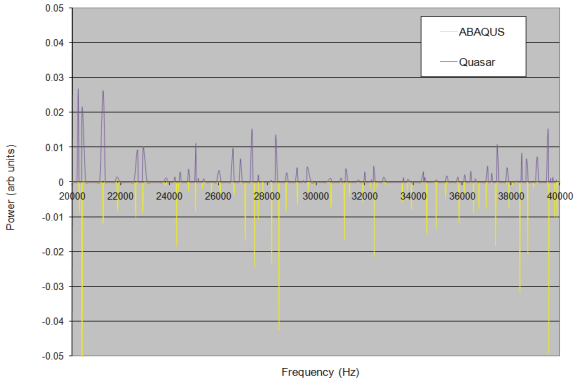

Figure 9. Steady-state dynamics comparison for the 20 kHz to 40 kHz resonance frequencies.

Conclusions

In this concept feasibility study, we have demonstrated that it is not only possible to use finite element-based frequency extraction to predict the vibrational frequency of a simple part, but it is also possible to predict the vibrational frequency as well as the mode shape of a complicated, production-level part with very good accuracy. With the rapid development of computer hardware and software, finite element analyses and perturbation analyses will be capable of putting RI on a more science-based quantitative basis.

It is commonly acknowledged by the original equipment manufacturer (OEM) participants that the work completed in this project is of greater magnitude and quality than expected. Unexpected computational capabilities have also been shown and investigated. Based on what has been achieved, a follow-on technical feasibility study has been proposed and approved by USAMP in developing an industry-wide standard and the associated sorting modules for computationally enhanced RI.

References

1. X. Sun and M. H. Jones, "NDE 701 – Enhanced Resonance Inspection for Light Metal Castings," US-DOE Automotive Lightweighting Materials, FY2007-2008 Annual Progress report.
2. C. Dasch, X. Sun, C. Lai, J. Saxton, G. Stultz, G. Palombo, C. Grupke, G. Harmon, L. Ouimet, D. Simon and M. Jones. Towards Quantitative Resonance Inspection: Resonance Mode Identification and Modeling, Proceedings of Review of Progress in Quantitative Nondestructive Evaluation, Chicago, Illinois, 2008.
3. C. Lai, X. Sun, M. Jones, C. Dasch and G. Harmon. Project Final Report - NDE 701- Enhanced Resonance Inspection for Light Metal Castings. Pacific Northwest National Laboratory, Richland, WA. PNNL-18630, July 2009.
4. ABAQUS, 2007. Analysis User's Manual. Version 6.7.

Presentations/Publications/Patents

1. "NDE 701: Enhanced Resonance Inspection for Light Metal Castings," AMD Offsite, Southfield, Michigan, Oct 29, 2008.
2. C. Dasch, X. Sun, C. Lai, J. Saxton, G. Stultz, G. Palombo, C. Grupke, G. Harmon, L. Ouimet, D. Simon and M. Jones. Towards Quantitative Resonance Inspection: Resonance Mode Identification and Modeling, Proceedings of Review of Progress in Quantitative Nondestructive Evaluation, Chicago, Illinois, 2008.

E. Concept Feasibility of Global Quality Assurance of Joining Technology for Automotive Body-in-White

Principal Investigator: Xin Sun
Pacific Northwest National Laboratory
P.O. Box 999, Richland, WA 99352
(509) 372-6489; e-mail: xin.sun@pnl.gov

Industry Consultants: Ford, General Motors, Chrysler

Technology Area Development Manager: William Joost
(202) 287-6020; e-mail: william.joost@ee.doe.gov

Field Technical Manager: Mark T. Smith
(509) 375-4478; e-mail: mark.smith@pnl.gov

Contractor: Pacific Northwest National Laboratory
Contract No.: DE-AC05-76RL01830

Objective

- To quantitatively evaluate the effects of missing bondline or missing welds on the global resonance signature of an automotive body-in-white (BIW).
- To assess the feasibility of a new inspection technique that will provide a global quality factor of the joining technology used for an automotive BIW.

Approach

- Evaluate the sensitivity of resonance spectroscopy to detect defects such as a partial weld or an improperly cured adhesive in a simple structure.
- Determine target values for sensitivity, reference surrogates of defects, and functional requirements to be acceptable in a manufacturing environment and compatible with either inline or offline quality assurance and cost targets to ensure an inspection is economically affordable for the manufacturer.
- Determine techniques of exciting vibrational modes and other methods of stimulus that will intentionally stress a predetermined region to increase sensitivity to a selected site.
- Investigate novel means to reduce implementation cost.
- Determine advantages, technology gaps, and implementation issues; investigate cost-effective means for implementation at automotive assembly plants and define paths for future development.

Milestones, Metrics, and Accomplishments

Milestone 1: Report of Concept Feasibility Study of Global QA of Joining Technology for Automotive BIW. Completed September 2009 (PNNL-18838).

Accomplishments

- Fabricated adhesively bonded generic hat sections: perfectly bonded and with intentionally missed bondlines. Experimentally measured the resonance spectra for all the three part populations using resonance inspection (RI).
- Performed statistical data analyses on experimentally obtained RI data to demonstrate the concept feasibility of using RI in detecting lack of bonding in automotive BIW-level parts.
- Determined advantages, technology gaps, and implementation issues.

Future Direction

- The project has been completed.
- The success of this concept feasibility project has led to the development of a new project proposal on technical feasibility of Global Quality Assurance of Joining Technology for Automotive Body-in-White.

Introduction

While the domestic automotive industry continues to introduce new lightweight materials and associated joining technologies to body-in-white (BIW), the need emerges for a global quality assurance tool that is nondestructive and able to quickly evaluate the joining technology for an entire automotive BIW. Current practices employ statistical testing with destructive measurements that are labor-intensive, ergonomically unfriendly, costly, and time intensive. Further, continuous joints such as adhesive bonds or laser welds can be difficult to inspect destructively, and joints in high-strength steel can be too strong to be pried apart.

Facing these challenges, this project will examine the concept feasibility of using a global joint quality evaluation and assurance approach by quantifying the contributions of joint integrity (discrete as well as continuous) to the overall structural stiffness of the BIW through vibration mode and natural frequency analyses. The proposed method is computationally intensive and examines BIW natural frequency and vibration modes using structural finite element analyses. Different means of structural excitation and effects of different boundary conditions will be established by detailed finite element structural/modal analyses on BIW models provided by the original equipment manufacturers.

Partnering with automotive manufacturers is critical to ensure the techniques of straining the BIW and performing three-dimensional (3D) imaging is conducive to a manufacturing environment and existing online production practices. Various experimental measurements including resonant spectroscopy and whole-body strain measurements using techniques such as shearography (shearing speckle interferometry) will be used as experimental model validations.

The proposed techniques are capable of whole body imaging, where either static or dynamic stress is applied and displacement is quantified on the order of nanometers. Comparing analyses results, the 3D displacement measurements will show a characteristic pattern when joining methods have been properly used and permit an objective means of evaluating quality.

The objective of the project is to assess the feasibility of a global inspection technique for the various joining technologies used for an automotive BIW. Three component-level parts have been examined in this concept feasibility study: welded strips, bonded strips, and bonded hat sections.

Our FY08 annual report (Sun et al. 2008) summarizes the resonance inspection (RI) results for the welded and bonded strips populations. In FY09, we focused on a generic hat section to evaluate the feasibility of using a global measurement technique, such as RI, to determine the bond quality of a BIW level part. The fabrication process and corresponding resonance spectra of controlled good and bad parts in this population are detailed in this report. Conclusions and suggestions for future research will be made after the results are analyzed. More detail on sample fabrication procedures, measurement techniques, measured RI spectra, and data analyses procedures can also be found in our project final report (Sun et al. 2009).

Fabrication of Adhesively Bonded Hat Sections

Adhesively bonded hat sections are designed and fabricated to test the effectiveness of using resonance spectra to discriminate lack of bonding parts from fully bonded parts.

Figure 1(a) schematically illustrates the dimensions of the idealized, generic hat section. The top hat and the base plate are made of 1.2-mm gage mild steel sheets. Note that these parts were accurately cut and bent in the machine shop at Pacific Northwest National Laboratory, and they do not have the typical production line part-to-part variations observed in the automotive production environment. Figure 1(b) shows a typical hat section as fabricated.

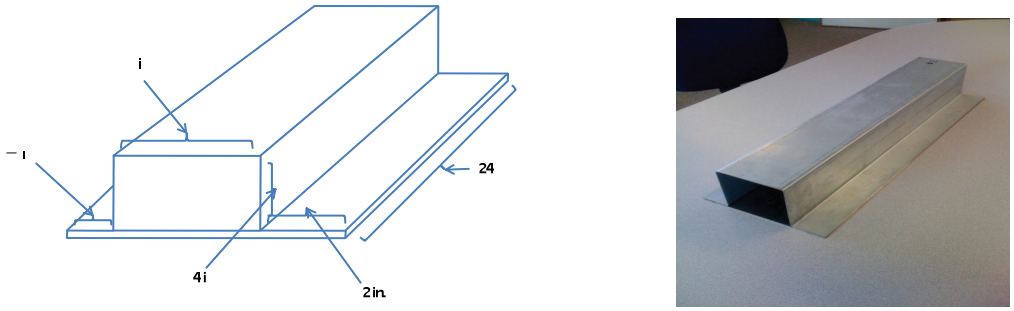

(a) (b)

Figure 1. Illustration of adhesively bonded hat section.

The structural adhesive Dow Betamate 73305GB was used in the bonding process. In total, six bonded hat sections were fabricated and cured under vacuum condition. Two sections (G1 and G2) were perfectly bonded with 24-in. bond lines on both flanges. The remaining four "bad" samples (G3-G6) were made with intentionally missed 8-in-long bond lines at various locations on the two flanges.

Resonance Spectroscopy Measurements

The Modal Shop (TMS) hammer impact system was used to measure the resonance spectra of the six bonded hat sections. The experimental set up is shown in Figure 2. Two 1-in.-wide nylon rails were positioned 2 in. away from both ends of the parts as supports. The impact point was at the center of the part (12 in. from either side, or 2 in. up/down from the top).

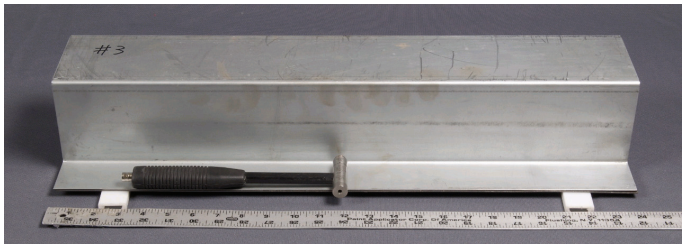

Figure 2. TMS resonance test set up.

Figure 3 (a)-(f) shows the measured resonance spectra for the two good parts (G1 and G2) in different frequency ranges. The results shown in Figure 3 clearly demonstrate that discrete resonance peaks can be measured for the adhesively bonded hat sections. That is, the bonded hollow sections ring and the attenuating effect of the adhesive are not dominating in the resonance spectra for the hat section as was seen in the adhesively bonded strips (Sun et al. 2008). In addition, the test results shown in Figure 3 indicate that the resonance spectra comparison between the two good parts share many similar resonance peaks. This is particularly true for frequencies of less than 15 kilo-Hertz (kHz). In the frequency range >15 kHz, their resemblance decreases. This may be due to the small number of measurements and the high noise-to-signal ratio for this measurement technique at higher frequency ranges.

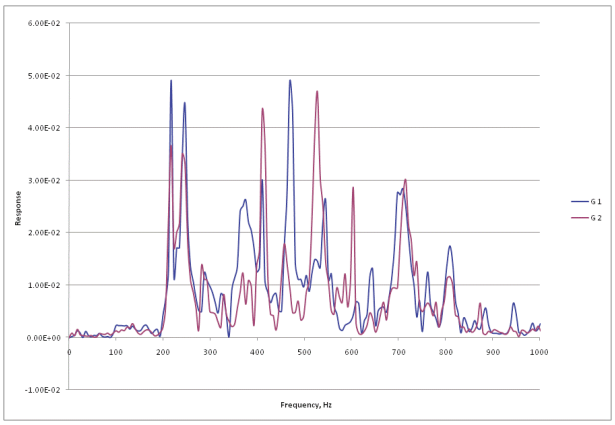

(a) 0-1,000Hz

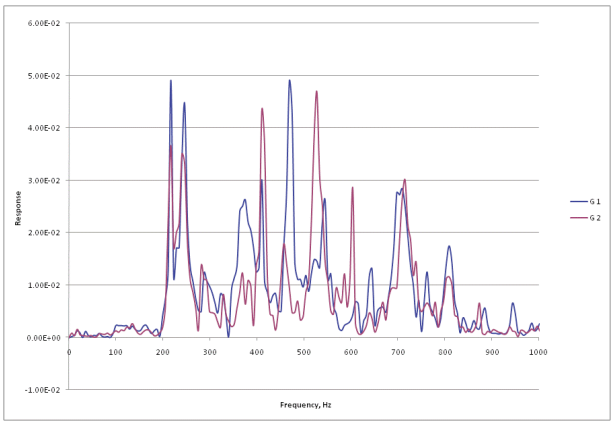

(b) 1,000Hz-2,000Hz

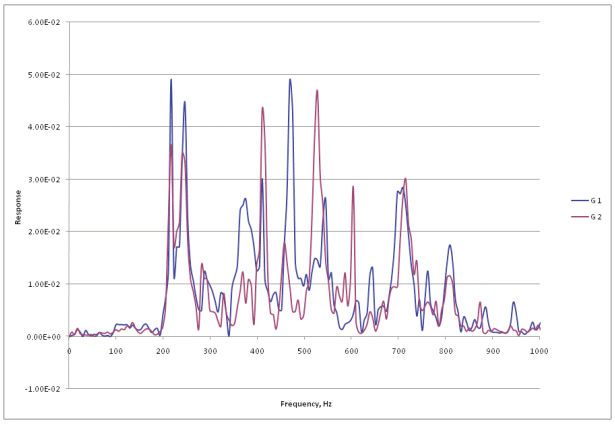

(c) 2,000Hz-5,000Hz

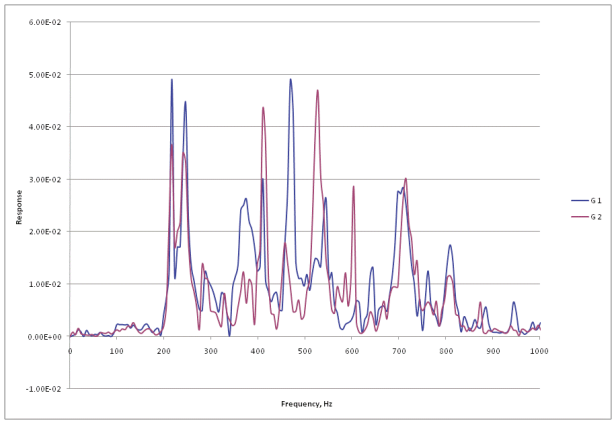

(d) 5,000Hz-10,000H

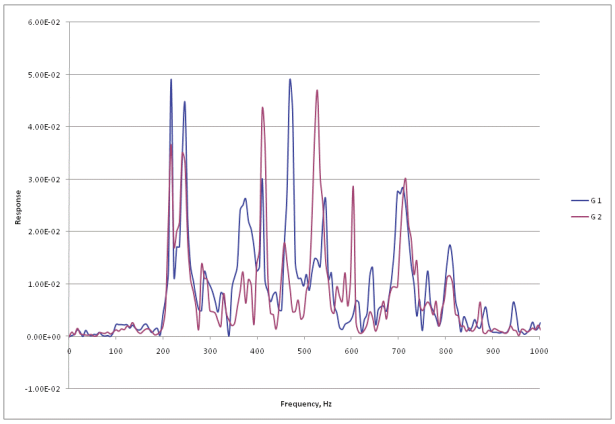

(e) 10,000Hz-15,000Hz

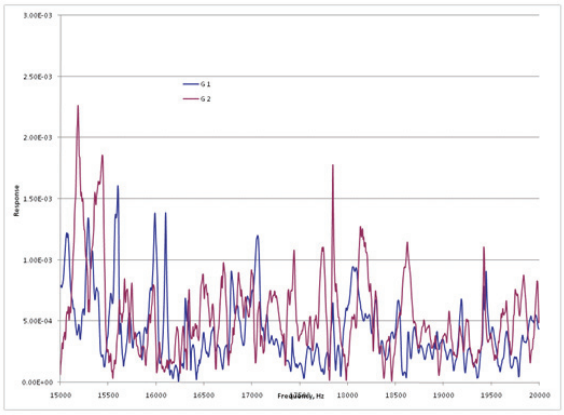

(f) 15,000Hz-20,000Hz

Figure 3. TMS measured resonance spectra comparison for the two good hat sections

Figure 4 shows a typical spectra comparison between the good part (G1) and a bad part (G3-missing an 8-in. bond line on the 2-in-wide flange). The results here indicate that the bad part is missing many distinct resonance peaks compared to the good part, particularly in the frequency range of 3 to 7 kHz. At higher frequency ranges, i.e., >10 kHz, some significant frequency shifts are also observed between the two parts.

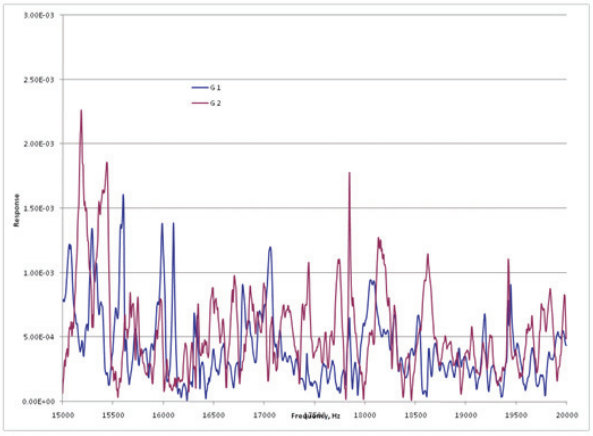

(a) 0-1,000Hz

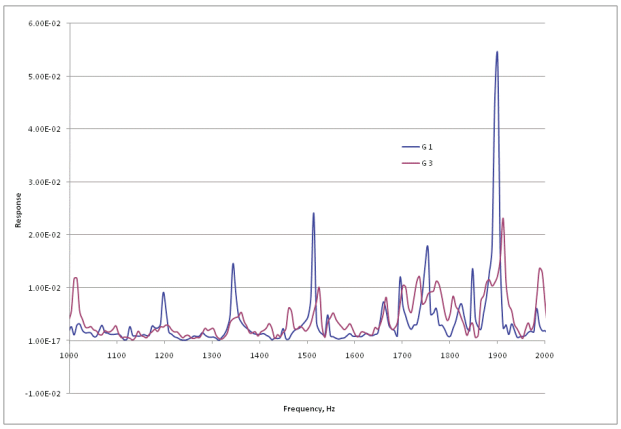

(b) 1,000Hz-2,000Hz

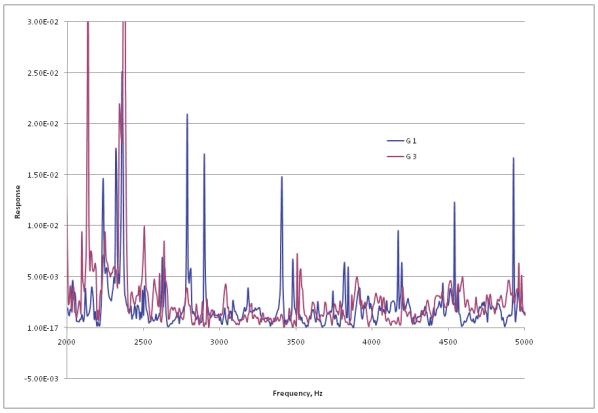

(c) 2,000Hz-5,000Hz

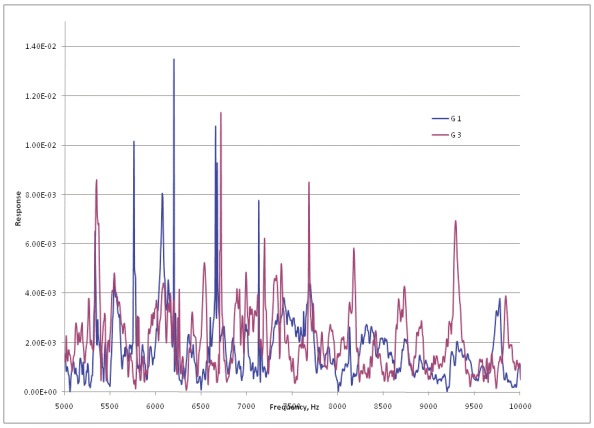

(d) 5,000Hz-10,000Hz

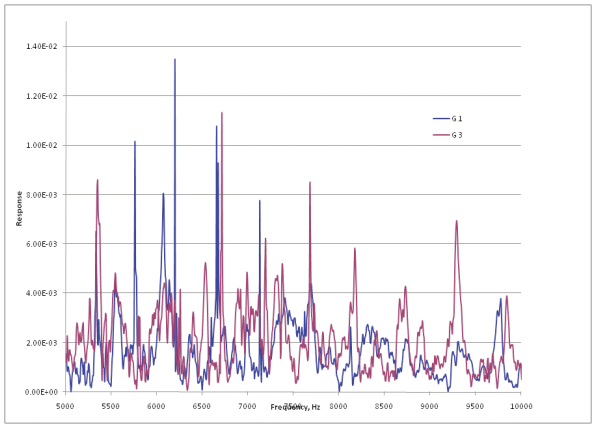

(e) 10,000Hz-15,000Hz

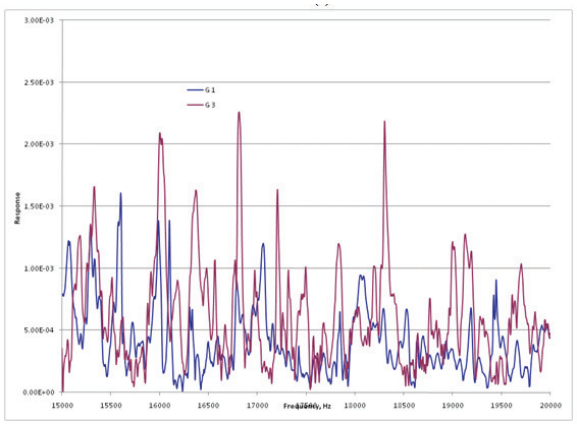

(f)15,000Hz-20,000Hz

Figure 4. TMS measured resonance spectra comparison between a good part (G1) and a bad part (G3)

These results are very encouraging in the sense that: 1) a clear resonance pattern can be established for the good parts, and 2) clear resonance differences can be observed between the good and bad part. Spectra comparisons for all the other parts are processed and stored in Excel™ format. They show the same trends as discussed above.

Statistical Data Analyses with Test Statistics

This section summarizes the preliminary results of a statistical data analysis using the resonance spectra measured for the adhesively bonded hat sections. The problem was formulated as a classic discrimination problem. First, the spectra for all the bonded hat sections are used to establish the test statics for the bonded hat section population. The detection statistic is expressed in a weighed sum of the spectrum:

$$D(P) = \sum_{i=1}^{n} W_i P_i$$

with the weights determined by the means of the good and debond samples:

$$W_i = \frac{Mean(P_i \mid debond) - Mean(P_i \mid good)}{Mean(P_i \mid debond) \bullet Mean(P_i \mid good)}$$

The detector is produced by thresholding the test statistic, T. That is, if $D(P)<T$, then classify the part as good, and if $D(P)>T$, then classify the part as bad. The threshold value, T, is set to produce a specific false call probability for detection. Practically speaking, the wider the range of effective T, the better the test statistic.

The mathematical details of the procedures for this statistical approach are summarized in Sun et al. (2009). Figure 5 shows the receiver operating characteristic (ROC) curve for the good parts versus the debond part using this test statistic. The ROC curve is a statistical tool to display all possible probability of detection (POD) versus false call probability (FCP) values that can be achieved by the inspection method. Different POD and FCP performance is achieved by varying the detection threshold of the test statistic.

For example, if T is set at 1100 as shown in Figure 5, then the POD of the debonded parts approaches 1.0, and the false call probability of the good parts is almost 0. The results shown in Figure 5 clearly indicate that a threshold value, T, can be established such that the good parts can be distinguished from the bebond parts without ambiguity.

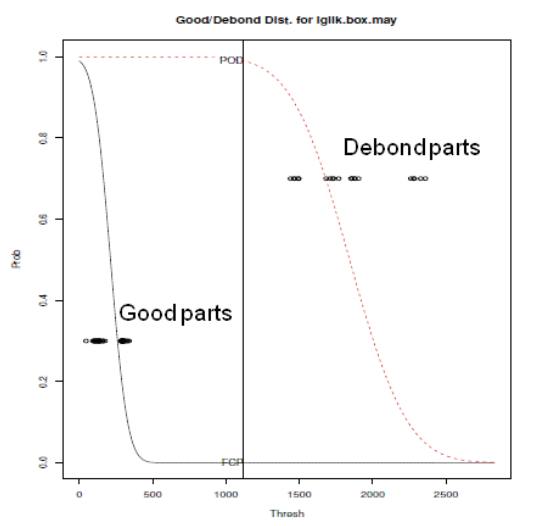

Figure 5. ROC curve of the hat section population

The conclusions from these statistical data analyses are:

- For the population of parts investigated in this study, it is possible to discriminate between good and debonded parts with little misclassification error.
- The good part populations, however, are very homogeneous and probably are not typical of production line parts.
- The debonded parts differ from the good parts significantly.
- Defects result in complex changes to the resonance frequency spectra.

Conclusions

The ability to use RI for detecting lack of bonding and/or subsized/missed spot welds in an automotive BIW has long been desired. The RI technique is quick and very sensitive, making it an ideal choice in production environments. This concept feasibility project set out to determine if it is feasible to accomplish this goal. The results in this study clearly demonstrate that:

1. RI is not effective in detecting lack of bonding in a fully bonded panel or strip due to the attenuating effects of the adhesive layer.
2. For the bonded hat sections and spot welded strips, it is possible to discriminate between good and debonded parts with little misclassification error based on the resonance spectra.
3. Defects result in complex changes to the response frequency spectra; spectra for the debonded parts differ from the good parts significantly.

The gaps and limitations of the current study are as follows:

1. The good part populations are very homogeneous and probably are not representative of production line part-to-part variations.
2. A larger population of good parts is needed for developing a more accurate algorithm and training.
3. Production-level part-to-part variations need to be considered in developing the detection algorithm.

4. Effective and consistent means of part excitation must be established.
5. Algorithms for inverse mapping must be developed such that given a resonance spectrum, the possible location of the lack of weld/bonds can be identified.
6. These gaps and limitations should be the focus of the next phase of study in evaluating the effectiveness of this technique in detecting production-level BIW parts.

References

1. 1. X. Sun, J.A. Carpenter and A.D. Yocum, “Concept Feasibility of Global QA of Joining Technology for Automotive Body-in-White (BIW),” US-DOE Automotive Lightweighting Materials, FY2008 Annual Progress report.
2. 2. X. Sun, C. Lai, P. Heasler, M.T. Smith and M. Good. Technical Report - Concept Feasibility of Global QA of Joining Technology for Automotive Body-in-White (BIW). Pacific Northwest National Laboratory, Richland, WA. PNNL-18838, September 2009.

F. Reliability Tools for Resonance Inspection of Light Metal Castings

Principal Investigator: Martin Jones
Nondestructive Evaluation Laboratory, Ford Motor Company
35750 Plymouth Road, Livonia, MI 48150
(313) 805-9184; e-mail: mjone147@ford.com

Technology Area Development Manager: William Joost
(202) 287-6020; e-mail: william.joost@ee.doe.gov

Contractor: United Sates Automotive Materials Partnership (USAMP[1])
Contract No.: DE-FC26-02OR22910

Objective

- To ensure the structural integrity of light metal castings by satisfying the need for rapid, reliable, in-line nondestructive evaluation (NDE).
- To develop a set of tools for resonance (acoustic) inspection (RI) that increases its reliability and robustness.
- To develop a set of software tools that can predict the probability of detection (POD) for a discrepancy given its type, size, orientation, and location when using RI. This set includes tools to predict accurately resonance frequencies in the absence of discrepancies, frequency shifts due to discrepancies, the normal frequency variability, and robust sort modules.
- To test the accuracy of the models on several commercial castings and to collect data on the time, manpower, and cost associated with heuristic and physics-based methods.
- To develop standard procedures to implement RI for production components and to ensure the accuracy, repeatability and traceability of the inspections.
- To research methods that may allow measured frequency shifts to determine the location, size, and type of discrepancies,

Approach including industrial partner/collaborator and path to technology transfer and commercialization

- Working with several casting vendors, make castings with a range of common discrepancies that can be quantified for each discrepancy type. These castings will be resonance inspected and then measured for strength to provide an RI-strength correlation.
- Working with RI system vendors, collect resonance spectra for the castings and develop sort modules using current heuristic methods.
- Working with finite element model (FEM) experts, create scalable models for the discrepancies and test their accuracy for predicting RI frequency shifts.
- Working with an acoustic system integrator, build an integrated work bench that allows RI to be evaluated beginning with only the CAD model and strength requirements of a part. This will use FEM to predict the resonances, predict POD for discrepancies, and optimize sort modules.

Milestone, Metrics and Accomplishments

- Commenced project and selected project vendors.
- Designed and resonance modeled a tensile bar that will be used to calibrate RI sensitivity to material strength
- Cast several batches of cylinders for the tensile bars with controlled levels of shrink porosity
- Collected and resonance inspected discrepant production castings from two different casters
- Translated ASTM E155 radiographic data[2] into physically dimensioned discrepancy sizes
- Began design of finite element program that will optimize selection of inspection resonance frequencies and predict the probability of detection.
- Drafted standardized process flow chart for developing RI plans for new parts
- Conducted a workshop on the need and requirements for a new acceptance standard for RI in production environments and developed an outline for the standard.

Future Direction

- During the next year, tensile bars with varying levels of porosity, crack size, and oxide inclusions will be cast, machined, resonance inspected, tomographed, pulled and micro-characterized.
- The results from the tensile bars will give sensitivity response curves and provide details to develop finite element models of the discrepancies.
- Traditional heuristic inspection plans will be developed for the tensile bars and the two production castings. These will provide a baseline to compare with the physics-based predictions.
- The framework for the physics-based FEM model will be coded and tested.
- A draft standard for production resonance inspections is to be completed.

Introduction

There are many automotive castings that are either safety or performance critical to the vehicle and require 100% inspection with extremely high requirements for the confidence of reliability. These include many chassis and powertrain components. Usually these have complex shapes and present extremely difficult inspection problems even with multi-view x-ray systems or surface-only inspections such as dye-penetrants.

Resonant (acoustic) inspection (RI) offers unique capabilities for these inspections. Sound in the range of 100 to 100,000 Hz can readily penetrate small to very large castings and is sensitive to heat treatment, porosity, cracks, and at least some oxide inclusions. Resonance inspection also has significantly lower capital and piece costs than either radiographic testing (RT) or fluorescent penetrant inspection (FPI). In fact, resonance inspection is already used for 100% inspection of many castings such as knuckles, rocker arms, master cylinders, and brake calipers. Figure 1 shows a schematic representation of a resonance inspection. To date, these resonance inspections have been based on heuristic sort modules. Sets of good parts and of

discrepant parts are used to select a set of inspection resonances (acoustic frequencies with associated frequency window) and to build sort rules that can separate the two sets of parts correctly (see Figure 2).

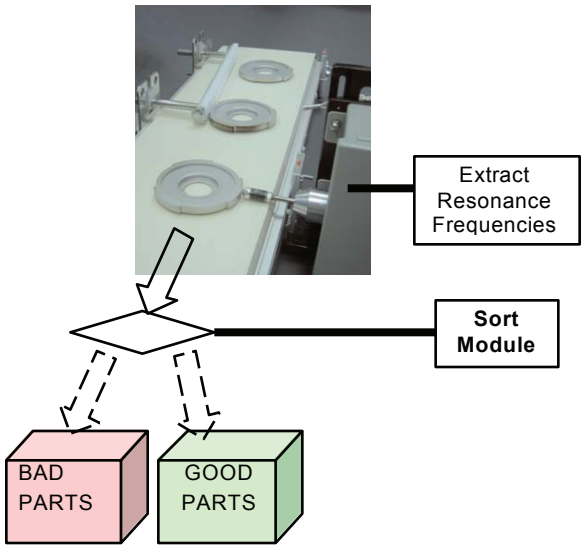

Fig. 1. Schematic representation of a resonance inspection.

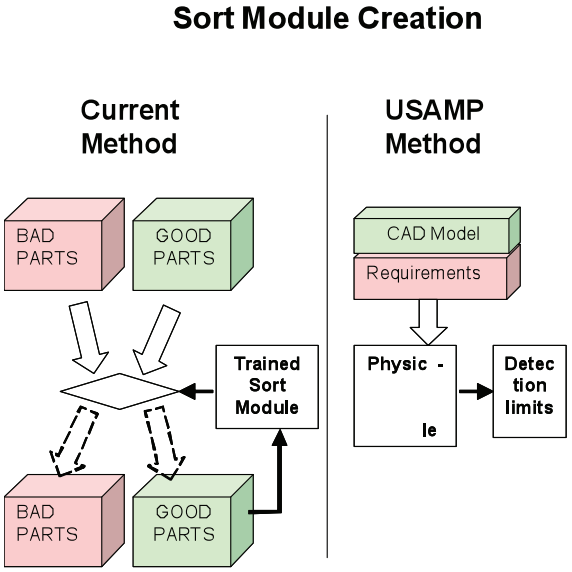

Figure 2. Schematic comparison of prior heuristic sort modules with new physics-based approach.

Despite these successes, resonance inspection has not been universally adopted for three sets of reasons.

1. The sensitivity of a given resonance inspection to a particular size discrepancy in a given location has been generally unknown. Rarely has the sensitivity been directly measured even for simulated discrepancies such as drilled holes or saw cuts. Nor can the sensitivity be estimated even by experts in the field. The physics of the resonance problem have been very underdeveloped compared with radiographic or ultrasonic inspections.

2. The second set of reasons involves the robustness of the inspection to allowed part variations. Castings of a part are almost always made with several cavities in several different molds. In addition to initial mold variations, the molds will experience wear as many parts are cast. The resulting castings will have small dimensional and processing condition variations. Frequently, heuristic sort modules must be rebuilt and re-verified as more molds and cavities are brought into production leading to uncertainty, reduced reliability, down time, and major expense.

3. There is not currently a resonance inspection standard that establishes a traceable inspection that can be used to support the reliability of a given inspection.

This project is designed to address each of these sets of problems. In general terms, the project is aimed at replacing the current heuristic approach with a priori or physics-based tools as seen in Figure 2. The project's deliverables are

1. Standardized procedure for RI in production

2. Integrated tools to predict probability of detection (POD) to critical defects

3. Software tools to create sort modules

4. Evaluate ability to identify anomaly type, size, and location from RI data

This project builds on the NDE701 project that demonstrated the technical feasibility of using FEM to accurately predict the resonance spectra of complex shapes such as front knuckle castings.[3] This new development project was approved in March of 2009 but the first purchase orders were not approved until September 2009. This report covers the progress that has been made on Tasks 1 to 4 during this period.

Integrated tools for POD to critical defects

This task is targeted at creating accurate probability of detection (POD) predictions for resonance inspection of the principal casting discrepancies. The discrepancies to be included are shrink porosity, cracks, and oxide inclusions. To predict the POD there are three essential ingredients: 1) the sensitivity of the response to the size of the discrepancy: for RI, the response is the frequency shift of a resonance due to the discrepancy; 2) the noise in the frequency shifts due all sources: these include measurement error (<1 part in 10,000) and resonance variability due to acceptable material variation (typically 1 part in 1000); and 3) the sort module selected.

1. Creating discrepancies

To determine the RI sensitivity (i.e. frequency vs. discrepancy size response), a set of simple samples with well-characterized discrepancies are being cast. These discrepancies will first be non-destructively inspected especially by computed tomography and resonance inspection. They will then be tensile tested to relate the effect of the discrepancy on the strength. Post facto, the discrepancy revealed by the tensile test will be analyzed with metallographic, fractographic, and micro-hardiness measurements. These measurements will then be used to create finite element models of standard, scalable discrepancies for shrink porosity, cracks, and oxide inclusions.

The simple shape selected for the discrepancy castings is a modified ASTM B577M5 tensile bar (see Figure 3) cast from A356 and given a T6 heat treatment. Tensile strength was chosen as the strength characterization since it can be run quickly and has been correlated to discrepancy size previously (Reference). A sample with a relatively large gauge size (12.5 mm dia.) was selected to make the RI simpler and to allow for variations in the locations of the discrepancies within the castings. The standard tensile bar was modified by removing small areas of the ends to make it asymmetric: this breaks modal degeneracies and simplifies the mode assignment.

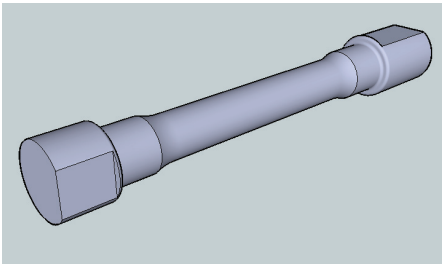

Figure 3. RI tensile bar design with 12.5 mm diam. gauge section.

Several different designs of the tensile bar were evaluated to ensure the design has sufficient asymmetry. The designs were tested using the FEM methods developed during the NDE701 project. There are three classes of modes associated with increasing stiffness: transverse bending, torsional, and longitudinal stretching. Examples of the first two modes of each type are shown in Figure 4. The predicted frequencies below 100 kHz are shown in Figure 5. The bending modes would normally be doubly degenerate with deflections at right angles to each other. The mode splitting between these bending modes, induced by the bar asymmetry, is indicated in the graph and ranges from 1 to 400 Hz.

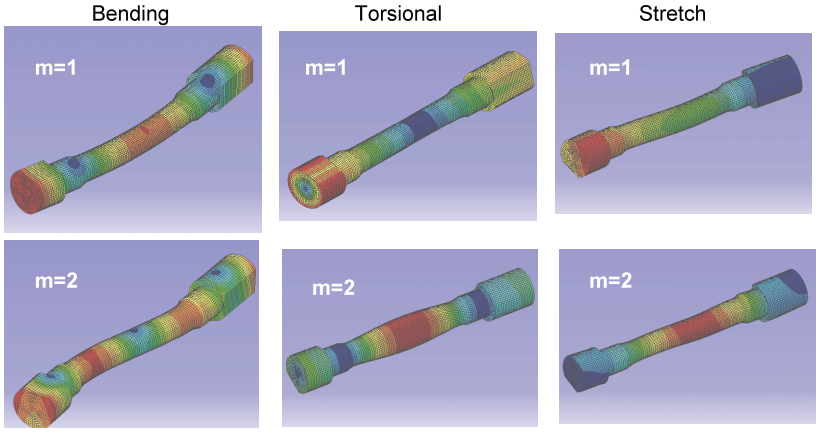

Figure 4. Representative resonance modes calculated for the modified ASTM B577 tensile bar. Only the lowest two modes of each class are included. Only one of the two nearly degenerate bending modes is included.

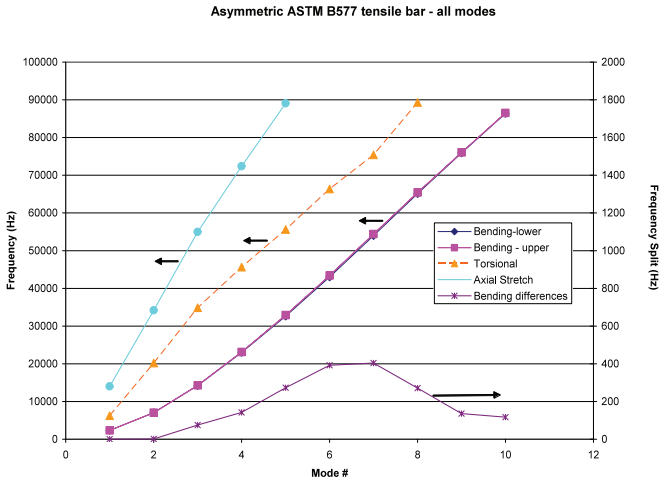

Figure 5. Predicted resonance frequencies for modified ASTM B577 tensile bar grouped by mode type.

A series of 54 cylindrical castings with three different diameters have been cast at the Chrysler Technical Center. The lower pattern used to make the mold for the sand castings is shown in Figure 6. These castings include both low and high shrinkage porosity samples.

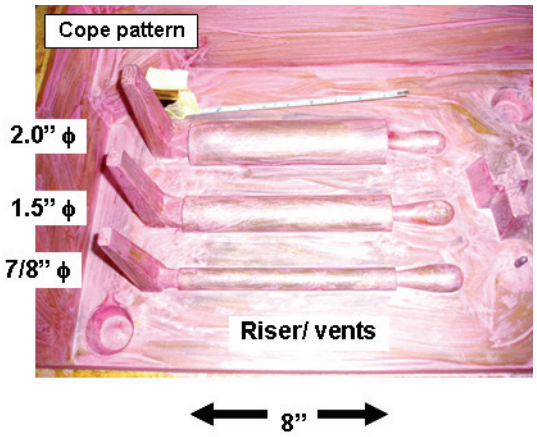

Figure 6. Lower pattern used to make cylindrical castings for tensile bars.

The castings have been x-rayed in two orthogonal views to establish the discrepancy size and location. Figure 7 shows illustrative radiographs of a good casting and a casting with a discrepant amount of shrink porosity. The shrink porosity includes both cavity and sponge types.

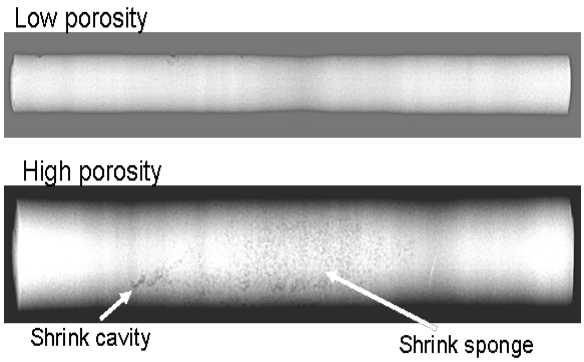

Figure 7. X-ray radiographs of porosity in two cylindrical castings.

In the next round of castings, oxide inclusions will be created. These will include both gross dross forms and film oxides.

To produce tight cracks, some of the good castings will be cycled at low tension in order to produce high-cycle fatigue cracks. It is planned that the cylinders will first be circumferentially notched to confine the crack to the middle of the bar. Then, a piezo-stack running at roughly 1000 Hz will be used to fatigue the bars. The cracks will be grown to varying depths. After crack growth, the outer surface will be machined away to remove the notches and define the gauge section.

2. Discrepancies found in production

In addition to the experimental discrepancies described above, production foundry discrepancies are being pulled for two parts produced by two of our casting participants. Both castings are produced with multi-cavity permanent mold processes. These discrepant castings are found by

normal quality assurance using x-ray, fluorescent particle, and visual inspections. This is a difficult task since discrepant castings are made infrequently. These are all resonantly inspected. Some of these will also be machined into tensile bars and tested for comparison with the experimental castings.

3. Calibrating discrepancy sizes

Safety critical castings such as some chassis components are typically 100% radiographically inspected following ASTM E155 or ASTM E2422. These standards use actual cast blocks that have a range of sizes for several discrepancy types (gas holes, shrink cavity porosity, shrink sponge porosity, high and low density inclusions). For each discrepancy type, the castings have been subjectively ranked or given a grade depending on the severity (size) of the discrepancies. Only by long experience has it been determined what radiographic grade is needed for each component. Part of these short comings arises because the sizes of the discrepancies in the radiographic standards have not been published.

In the USAMP/AMD "Design and Product Optimization for Cast Light Metals Project" completed in 2001 there was an activity at Lawrence Livermore National Lab to re-radiograph the ASTM E155 castings and to analyze those radiographs for discrepancy size. For the discrete discrepancies (gas holes, shrink cavities, and inclusions), the LLNL analysis included the projected area of the discrepancies, the maximum feature size, and an effective depth (from the calibrated attenuation measurements). Each of these measurements gives a different characteristic size.

The final step to reduce this information to a single dimension or size was never completed. We have re-analyzed this data for each of the different casting types for the discrete defects to determine if there is a consistent size that can be associated with each grade. Using either a circle equivalent diameter or a sphere equivalent diameter gave similar results. It was concluded that the area equivalent diameter is the most accurately measured property using ASTM E155 and provides the best scalar representation of the discrepant classes.

Finite element sort modules

To have a useful physics-based tool, it is necessary to integrate all the physics into a software tool bench. This will begin with the part design (CAD model) and the engineering requirements (peak loads and associated locations). These inputs then must be converted into finite element models for the part and for discrepancies that would limit the performance of the part.

These inputs and the other elements of the processing are shown schematically in Figure 8. The important physics that will be included are the sensitivity to discrepancy type, size, and location that was described above; efficient means to predict the frequency variability; and the efficient means to optimize the sort module and to include process compensation. Process compensation is the inclusion of some resonance lines to compensate for allowable geometry and material property variations.

These tools will be built within a commercial finite element environment maximizing the use of existing tools that are available for modal analysis.

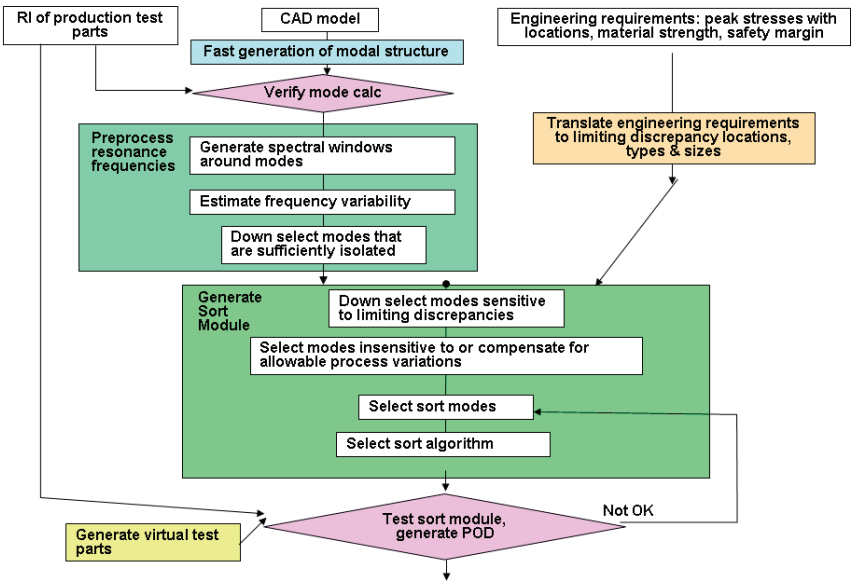

Figure 8. Inputs and data processing for the proposed FEM tool to create physics-based RI sort modules.

Standardized Procedures

The last task of the project is produce a standard that will lead to accurate, repeatable, and traceable inspections in the production environment. There already exists one standard6 for resonance inspection, but it is mostly a generic guide to the technology. There have been several OEM procedures drafted that address implementation procedures. These have been synthesized into a standard process flow chart. This will be used for the creation of sort modules for the three castings being tested in the project.

Despite these documents, there is a gap in the available standards and procedures relevant to making production inspections reliable, repeatable, and traceable. This gap includes the consistent use and documentation on 1) the inspection procedure used; 2) measurements on the repeatability and reproducibility; 3) the numbers and types of discrepancies used to measure the accuracy of the final sort module as well as the error rates for this validation set; and 4) preservation of results from production inspections.

In June 2009 a workshop was held to review the state of RI standardization and to propose the areas to be included in a new standard. The workshop concluded that this document is an essential element for productionizing RI.

Conclusions

Resonance inspection is a promising technology for ensuring the quality of light metal castings that require high reliability. This project addresses three of the technical barriers limiting the implementation of RI. These include the need for probability of detection predictions for given inspections, the need for more reliable sort modules, and the need for standard traceable inspection procedures. When completed, this project will deliver tools that are or are very close to being commercially ready.

Presentations/Publications/Patents

Dasch C, X Sun, C Lai, J Saxton, G Stultz, G Palombo, C Grupke, G Harmon, L Ouimet, D Simon, and M Jones. 2008. “Towards Quantitative Resonance Inspection: Resonance Mode Identification and Modeling.” Review of Progress in Quantitative NDE.

“NDE 901: Enhanced Resonance Inspection for Light Metal Castings.” 2009. AMD Offsite, Southfield, MI. October 13.

C. Lai, X. Sun, C. Dasch, G. Harmon, and M. Jones, “Quantifying Resonance Inspection with Finite-Element-Based Modeling”, submitted to J. Sound and Vibration, Oct. 2009.

References

1. Denotes Project 701 of the Nondestructive Evaluation Working Group of the United States Automotive Materials Partnership (USAMP), one of the formal consortia of the United States Council for Automotive Research (USCAR, www.uscar.org) set up by Chrysler, Ford and General Motors to conduct joint, pre-competitive research and development.
2. ASTM B155-05 “Standard Reference Radiographs for Inspection of Aluminum and Magnesium Castings.”
3. USAMP Project NDE701 “Enhanced Resonance Inspection for Light Metal Castings.”
4. See for example A. Migliori,and J. L. Sarrao, “Resonant Ultrasound Spectroscopy” (John Wiley & Sons, 1997) or J. He and Z Fu, “Modal Analysis” (Butterworth-Heinemann, 2001).
5. ASTM E577M “Standard Test Methods of Tension Testing Wrought and Cast Aluminum- and Magnesium-Alloy Products.”
6. ASTM E2001-08 “Standard Guide for Resonant Ultrasound Spectroscopy for Defect Detection in Both Metallic and Non-metallic Parts.”